

1 **RESPONSE TO ANONYMOUS REFEREE #1 COMMENTS (JUNE 2020)**

2 **Referee #1:**

3 **General Comment:** “Deep time climate and ecosystem reconstructions are challenging. Understanding
4 how Earth’s climate, tectonic and ecosystem modifications are linked represent an interesting advance.
5 Consequently, this paper is an important contribution. Overall the article is well written however the
6 discussion can be improved (not enough well organized). I identified several areas requiring
7 clarification (listed below). These problems being easily solvable, I recommend a minor revision
8 (ranked by order of importance).”

9 **Response:** We thank reviewer #1 for their appreciation of this work.

10
11 **Comment (1):** “The discussion is not very clear. Indeed short-term variations and long-term processes
12 are included in same sub-sections without to distinguish between modeling results and proxy (for instance
13 lines 191-225 introduce modeling results while lines 226-243 present short-term pCO₂ variations and
14 biological turnovers. I do not think this presentation is very clear for the reader, indeed these parts have
15 no links (or there is something lacking)). Moreover the discussion about ecosystem perturbations is
16 interesting but has a modest impact to understand links between paleo-pCO₂ and biological events. To
17 highlight their results, the authors may consider to split their discussion (long-term vs short term) or
18 creating a new sub-section for presenting modeling results.”

19 **Response:** We, respectfully, do not agree that the discussion needs to be reorganized. We chose to present
20 the discussion holistically by integrating modeling and proxy components via time increments. That is,
21 we present three segments that not only correspond to three climatically and ecologically unique intervals
22 (Middle to Late Pennsylvanian, Asselian and Sakmarian portion of the early Permian, and the remainder
23 of the early Permian) but also correspond to long term pCO₂ trends and important superimposed short-
24 term trends. We strongly feel that removing the short-term trends into a separate section results in loss of
25 context in relation to the long-term trends throughout the record.

26 That said, in order to resolve reviewer #1’s concern that short- and long-term term CO₂ variability and
27 processes are presented together in the discussion, we have reorganized the manuscript in the following
28 manner:

29 We have altered lines 226-227 (**lines 230-232** after changes suggested by reviewers 1 and 2) to “Short-
30 term fluctuations in pCO₂ are superimposed on the long-term decline through the latter portion of the
31 Carboniferous. These short-term fluctuations have been confirmed as statistically significant (99.9 to
32 100% of estimates; Fig. 4b-d) and coincide with major environmental and biotic events.” in order to
33 provide a better segue the switch from discussion of the long-term trends to the superimposed short-term
34 trends.

35 In addition, we have removed subsection 4.3 and rearranged and integrated that text into the latter portion
36 of subsection 4.2 (**lines 351-382** after changes suggested by reviewers 1 and 2). In this manner, all sections
37 in the discussion are now arranged by subsections that correspond to time and CO₂ trends. Each subsection
38 is structured such that the long-term proxy trends and model explanation of those long-term trends are
39 discussed first, followed by discussion of short terms trend and their correlation ecosystem perturbation.
40 This reconfiguration preserves the intended holistic presentation of the discussion while also clearing
41 delineating long- and short-term trends within each subsection. We hope that this resolves the issue
42 brought forth by reviewer 1.

43
44 **Comment (2):** “A few sentences of the discussion need to be rephrased or revised in order to reflect that
45 initiation and deglaciation CO₂-thresholds are different due to the climate hysteresis. Indeed the authors
46 tend to consider the “CO₂ glacial threshold” as an absolute value which determines the climate state of
47 the Earth. The line 299 is correct because the final pCO₂ (case at 270Ma, blue dote fig.5) is far above the
48 glacial threshold however elsewhere even if the simulated CO₂ overcomes the proposed glacial threshold,
49 that does not mean the termination of the Late Paleozoic Ice Age. ex : line 314 (the sentence can be
50 removed) ex : line 383-390 (this issue can be solved by adding error bars for age determination for each
51 steady state - indeed boundary conditions used to force climate models have their own uncertainties,
52 especially paleomagnetic data used to reconstruct paleographies)”

53 **Response:** We certainly did not intend to imply that the CO₂ threshold for initiation of continental ice
54 was a threshold above which all glaciers would collapse. Also on the time scales at which we are dealing
55 with in this paper (10s of thousands to millions of years), the time lag between the rise in CO₂ above a
56 level at which continental glaciers can be sustained and the timing of glacier collapse determined by
57 hysteresis (1000 of years) would not be discernable.

58 We have clarified the original statement (Line 314, **lines 335-339** after changes suggested by reviewers
59 1 and 2)) to address this by the following revision: “This finding, together with the hypothesized need
60 (the aforementioned mechanism two) for minimally a 4-fold increase in mafic-rock outcropping in order
61 to maintain CO₂ concentrations below the ice initiation threshold for a sustained period longer than that
62 of hysteresis (i.e., throughout the interval of minimum CO₂ and apex of glaciation; Fig. 5), argues for a
63 substantial increase in weatherability from the Carboniferous to early Permian driven by a compositional
64 shift in outcropping rocks available for weathering to a higher mafic-to-granite ratio.”

65 Concerning Lines 383-390 (**lines 401-409** after changes suggested by reviewers 1 and 2), we have added
66 error bars to simulated steady-state CO₂ and ⁸⁷Sr/⁸⁶Sr trendlines, constrained by the simulated intervals
67 (symbols on the figure) as requested.

68
69 **Comment (3):** “fig.3b. the chosen colour are misleading and implicitly suggests “anomalies”. Moreover
70 authors seem to assume two climate states characterized by a threshold close to 400ppmv of CO₂. This

71 point needs more explanation (why this threshold is so different compared to values used in fig.5 and
72 published by Lowry et al. 2014 ?)”

73 **Response:** The 400 ppm value is not a threshold, but rather the mean value for the 16 million-year record
74 of atmospheric $p\text{CO}_2$ through the later Pennsylvanian reported in Montañez et al. 2016 and was used here
75 as a guide solely. We have clarified this in the figure 3b caption (**lines 493-494** after changes suggested
76 by reviewers 1 and 2).

77

78 **Comment (4):** “line 167. I don’t understand how the duration of the “interglacial phase” has been
79 estimated (104 yr). S6 suggests a range of values for the sedimentation rate. Why the duration does not
80 seem to be affected by uncertainties (or explain why the duration does not depend on geological
81 parameters)? In addition could you precise if the proposed duration (104 yr) is the mean value or the
82 maximal value (or something else)? A brief paragraph summarizing limitations will be helpful for readers
83 not familiar with this method.”

84 **Response:** The Midcontinent and Appalachian cyclothems from which many of the samples were
85 obtained, are inferred as eccentricity cycles (Fielding et al. 2020). Fielding et al. 2020 has recently
86 concluded that “geochronological constraints are consistent with each cycle representing a 100 ky (short
87 eccentricity) interval, most likely related to waxing and waning of contemporaneous ice centers on
88 Gondwana.” In addition, given that interglacials of today have a duration of 10s of 1000s of years, by
89 analogy, interglacials of the past are also 10s of 1000s of years in duration. We have revised Lines 166
90 to 168 (**lines 167-171** after changes suggested by reviewers 1 and 2) to clarify this. The sentence now
91 reads: “Notably, the newly integrated record confirms elevated atmospheric CO_2 concentrations (482 to
92 713 ppm [-28/+72 ppm]) during Pennsylvanian interglacials in comparison to $p\text{CO}_2$ during glacial
93 periods (161 to 299 ppm [-96/+269 ppm]), with interglacial durations on the order of 1000s to 10s of
94 1000s of years given the inferred eccentricity scale duration of the glacial-interglacial cycles (Horton et
95 al. 2012; Montañez et al. 2016; Fielding et al. 2020).”

96 **RESPONSE TO ANONYMOUS REFEREE #2 COMMENTS (JUNE 2020)**

97

98 **General Comment:** “This paper improves the CO_2 proxy record for the late Paleozoic and compares CO_2
99 variations to other Earth system indices. Considerable care has been taken in assembling this record and
100 evaluating it statistically, which is much appreciated and it will be a useful resource for the community.
101 The paper also adapts previous modeling to assess what has driven the changes in CO_2 , and concludes
102 that a change towards more reactive silicate lithology is necessary, for which there is independent support.
103 Overall in my opinion it is a good, clear paper that needs little revision. I do have some minor revisions
104 to suggest.”

105 **Response:** We thank reviewer #2 for their appreciation of this work and encouraging comments.

106

107 **Comment (1):** “Line 39: typo “DiMichele, 2104”

108 **Response:** This has been fixed.

109

110 **Comment (2):** “Line 67: note the DOI address here does not currently work”

111 **Response:** This was intentional. The underlying data has been deposited in the Dryad Digital Repository,
112 but we chose to keep the data private during the process of peer review. If this work is accepted, we will
113 make the data fully public. Until that time, the data set can be shared privately via a URL if requested by
114 either the editor or reviewers.

115

116 **Comment (3):** “Line 78: it is a bit confusing that this paper appears to cite itself? Again on line 137.”

117 **Response:** That is not a citation of this paper, but the underlying data. The author guide to Climate of the
118 Past mandates “the proper citation of data sets in the text and the reference list (see section references)
119 including the persistent identifier.” We have cited the dataset as Richey et al. 2020 to comply with these
120 instructions. However, we have altered all of the in-text citations of the dataset to include the DOI and
121 make it clear that the dataset is being cited (**lines 74, 79, 82, 138, 478** after changes suggested by reviewers
122 1 and 2). If we have misunderstood the instructions on how and when to cite the underlying data, please
123 let us know and we will make any necessary changes.

124

125 **Comment (4):** “Line 112: Estimates of mean annual temperature are used to help determine past CO₂
126 levels. Any circularity should be considered here when going on to link the CO₂ estimates to climate.”

127 **Response:** Yes, this is correct; we used mean annual air temperatures as input for the PBUQ model to
128 estimate the paleo-CO₂ estimates in cases where the paleosol estimates were reformulated in this study.
129 For the part of the paleosol-based reconstruction that comes from Montañez et al. 2016 (i.e., the
130 Pennsylvanian and earliest Permian estimates), a broad range of temperatures of 20 to 26°C (i.e., 23°C
131 ±3°) was prescribed. For the estimates from Montañez et al. 2007 reformulated in this study (most
132 Permian paleosol estimates), we use proxy soil temperatures that come from many of the same paleosols
133 (Tabor and Montañez 2005; Tabor et al., 2013). For the latter, for intervals with proxy soil temperatures
134 of > 30°C, we used temperatures 5°C lower as the MAAT, for proxy soil temperatures of >25°C to ≤
135 30°C, we used temperatures 3°C lower, and for temperatures ≤ 25°C, we used the actual proxy value.
136 This scheme resulted in MAAT temperatures that range from 23 to 30°C. The error on these temperatures
137 was assigned at ±3°C, like the estimates from Montañez et al. 2016. Despite the differences in the method
138 by which MAAT was prescribed or calculated, out of the 103 paleosol-based estimates, only 5 MAAT
139 values used fall out of the range of 20 to 26°C (i.e., 23°C ±3°).

140 These MAAT estimates are purposefully broad, given the uncertainty in paleo-temperatures for these past
141 periods. However, the temperature ranges overlap with the range (18 to 26°C) indicated by the climate
142 modeling for the terrestrial realm of the Pennsylvanian and early Permian Pangaeian tropics (Poulsen et

143 al. 2007; Montañez and Poulsen, 2013; Macarewicz et al. in revision (*EPSL*). In addition, the
144 temperatures used overlap with the lower range of the pedogenic phyllosilicate temperatures (23 to 32°C)
145 published by Rosenau and Tabor (2013). Importantly, there is no circular reasoning involved in using
146 these values, as the reviewer raised as a concern, as these temperature estimates of 20 to 26°C encapsulate
147 the minimum and maximum temperatures simulated by a GCM (GENESIS3; Horton et al. 2010; 2012)
148 and an Earth System Model (iCESM 1.2; Macarewicz et al. 2019; in revision) for the continental tropics
149 over a CO₂ range of 280 to 840 ppm (overlapping the range of CO₂ calculated in the LOESS analysis in
150 this study (175 to 750 ppm). Thus, by using the full range of MAATS (20 to 26°C, rarely >26°C)
151 consistently throughout the modeling of the samples of Pennsylvanian and earliest Permian age, we feel
152 we have conservatively represented the realistic MAATs in the paleotropics during the late Paleozoic in
153 a manner that precludes circularity.

154

155 **Comment (5):** “Line 118: The Donnadieu paper cited is about the Cretaceous? Surely the model runs are
156 not from that work?”

157 **Response:** The Donnadieu et al. 2016 paper was solely referenced for the model and methods – not the
158 results. However, after review, we have decided that Donnadieu et al. (2006) would be a more
159 appropriate citation for model and methods than Donnadieu et al. (2016). We have addressed this
160 removing Donnadieu et al. (2016) and adding “and approach as described in Donnadieu et al. (2006).”
161 to the statement. The revised sentence now reads “The spatial distributions of the mean annual runoff
162 and surface temperature were calculated offline for five time increments (Goddéris et al., 2017)
163 covering the period of interest and for various atmospheric CO₂ levels using the 3D ocean-atmosphere
164 climate model FOAM and the approach as described in Donnadieu et al., (2006) (**lines 117-119** after
165 changes suggested by reviewers 1 and 2).

166

167 **Comment (6):** Line 170: “307 and 304.5 Ma” should read “307 until 304.5 Ma”?, “<400 to ←200 ppm”
168 also a bit confusing.

169 **Response:** This has been changed to “...2.5-Myr interval (307 to 304.5 Ma) of minimum CO₂ values
170 (less than 400 to as low as 200 ppm)...” (**line 173** after changes suggested by reviewers 1 and 2).

171

172 **Comment (7):** Line 173: missing subscript in CO₂

173 **Response:** This has been fixed (**line 176** after changes suggested by reviewers 1 and 2).

174

175 **Comment (8):** Line 269: “Notably, the 10-Myr pCO₂ nadir raises a paradox as to what was the primary
176 CO₂ sink(s) at the time given that the CO₂ sinks of the Pennsylvanian were no longer prevalent. This
177 paradox reflects the waning denudation rates of the CPM by the early Permian”. Note that Joshi et al.
178 (2019) in GRL have run climate model simulations for the earliest Permian and find higher silicate
179 weathering rates as the denudation rate wanes. They argue that denudation rates are not a strong control

180 on silicate weathering in mountains where the rate is high. Perhaps a weaker relationship between
181 denudation and silicate weathering may help explain the paradox identified here?

182 **Response:** We thank reviewer 1 for bringing to our attention this very important paper. Indeed, Joshi et
183 al.'s (2019) modeling results would support the idea of a delayed capacitor-discharge mechanism as the
184 origin of the long-term decline in $p\text{CO}_2$ through the last 16 Myr of the Carboniferous (in our record) from
185 ~500 ppm to <300 ppm by the earliest Permian, as well as the return to rising $p\text{CO}_2$ (to >500 ppm) after
186 10 million years into the early Permian.

187 However, we think that we must delve deeper into the respective models. The main improvement of Joshi
188 et al. (2019) compared to GEOCLIM is higher spatial resolution. The model used by Joshi et al. (2019)
189 allows a better representation of runoff, and hence, weathering, especially in the Central Pangean
190 Mountains (CPM). However, the major difference between both models is the absence of climate
191 dependence in the calculation of the spatially resolved physical erosion in Joshi et al. (2019). In their
192 model, physical erosion is only dependent on the prescribed altitude of each grid cell, meaning that
193 physical erosion is an external forcing of the model. This has major implications for the results of the
194 Joshi et al. (2019) model. Indeed, when the CPM are high, the drop in temperature limits weathering rates,
195 without compensation by enhanced runoff linked to orographic impact on the atmospheric circulation.
196 Consequently, in the Joshi et al. (2019) model, the maximum weathering is reached when the mountains
197 are already eroded (due to temperature rise at lower altitude), but physical erosion is also a function of
198 runoff. In GEOCLIM, the dependence of the physical erosion on runoff does not allow the existence of
199 such a delay between the maximum altitude of the CPM and the lowest atmospheric CO_2 .

200 Thus, we have a new paragraph to address this in Section 4.2 An Early Permian CO_2 Nadir (see **lines 284-**
201 **304** after changes suggested by reviewers 1 and 2). We hope that this change provides a balanced
202 discussion of our and Joshi et al., (2019) work. The new paragraph reads:

203 “Two mechanisms have the potential to resolve this paradox. The first, referred to as a delayed climate-
204 controlled capacitor (Joshi et al. 2019), leads to a multi-million-year delay between the timing of peak
205 orogenic uplift and maximum chemical weathering potential and CO_2 drawdown due to substantial
206 differences in chemical weathering rates during the different phases of an orogenic cycle. In their study,
207 the highest intensity of chemical weathering and capacity for CO_2 consumption occurs when mountains
208 have been somewhat denuded rather than during peak uplift, reflecting the disproportionate influence of
209 runoff temperature over hydrology and erosion on weathering potential. Notably, Joshi et al.'s (2019)
210 coupled climate and geochemical modeling of the Late Paleozoic Ice Age yield an evolution of simulated
211 $p\text{CO}_2$ over the period of uplift and denudation of the CPM that corresponds both in absolute CO_2
212 concentrations and magnitude of change over this period (~320 to 290 Ma). That said, in Joshi et al.
213 (2019), the physical erosion parameter is not dependent on climate, but, rather, is defined by the prescribed
214 altitude. Thus physical erosion is an external forcing in their model. The absence of runoff dependence
215 for physical erosion (as is the case for GEOCLIM) and the strong dependence of weathering on
216 temperature may be the trigger for their simulated delay between maximum uplift and the highest intensity
217 of CO_2 consumption by silicate weathering. In GEOCLIM, the dependence of the physical erosion on

218 runoff does not allow for a millions of years delay between maximum uplift of the CPM and lowest
219 simulated $p\text{CO}_2$. Further study is needed to interrogate the influence of this approach on the results.

220 The second mechanism, proposed here, is a substantial shift in the ratio of mafic-to-granite rocks
221 available for weathering from the latest Carboniferous to the early Permian. This reflects the doubling
222 or greater increase in weatherability of mafic mineral assemblages over granitic assemblages (Gaillardet
223 et al., 1999; Dessert et al., 2003; Ibarra et al., 2016), thus enhancing weathering efficiency and CO_2
224 drawdown, and creating a tighter coupling between CO_2 and climate. In turn, with tighter coupling
225 between CO_2 and climate, the global silicate weathering flux needed to maintain homeostatic balance in
226 the carbon cycle for a given scenario can be attained at a lower $p\text{CO}_2$ level.”

227

228 **Comment (9):** Line 284: The comparison to Macdonald et al. is a little different in timing: their suture
229 length reconstructions are small after 300 Ma.

230 **Response:** We are not sure whether we have misunderstood this comment. We agree that the compilation
231 of suture zones made by Macdonald et al. (2019) indicates that the ~10,000 km long Hercynian arc-
232 continent suture zone (in the paleotropics) was at a peak prior to 300 Ma (transition from Carboniferous
233 to Permian). Lines 286–289 (lines 308-310 after changes suggested by reviewers 1 and 2), state that we
234 used GEOCLIM to test the Macdonald et al. 2019 hypothesis that the influence of increased mafic
235 (ophiolites in their study) on $p\text{CO}_2$ was greatest in the *Carboniferous*. As well as to “to evaluate the
236 potential of increased weatherability, provided by increasing the ratio of outcropping mafic rocks to
237 granite rocks available for weathering, as the predominant driver of *the early Permian* CO_2 nadir. We
238 may have confused the reader by referring to both goals of the modeling in this section.

239 This has been resolved by revising the sentence (lines 308-310 after changes suggested by reviewers 1
240 and 2) to read “Here, we used the GEOCLIM model to, first, interrogate this Carboniferous hypothesis
241 further and, second, to evaluate the potential of increased weatherability, provided by increasing the ratio
242 of outcropping mafic rocks to granite rocks available for weathering, as the predominant driver of the
243 early Permian CO_2 nadir.”

244

245 **Comment (10):** Line 306: “rapid (0.000043/Myr)” use standard form here perhaps?

246 **Response:** This has not been changed as we believe the reviewer was asking that we change Myr to Ma.
247 However, this would be incorrect as Ma is for a specific time vs. Myr for an increment of time (here 1
248 million years).

249

250 **Comment (11):** Line 319: “our modeling results indicate that this is not compatible with proxy inferred
251 moderate surface conditions of the late Carboniferous” I would imagine many of the model parameters
252 are not known well enough to really rule this out? Perhaps a more tentative statement here?

253 **Response:** We very much appreciate the reviewer’s comment and we agree that the model parameters are

254 associated with uncertainty. The results that we refer to in this section of the Discussion (Lines 284-328,
255 **lines 305-339** after changes suggested by reviewers 1 and 2) are 1st-order differences in steady-state $p\text{CO}_2$
256 that would lead to climate regimes, which differ remarkably from one another. For example, the modeled
257 steady-state $p\text{CO}_2$ for a 2- to 4-fold increase in the surface outcropping of mafic rocks available for
258 weathering in the Pennsylvanian leads to near Snowball Earth conditions, which are incompatible with
259 other earth system conditions at that time (from the literature). Conversely, modeling with the reference
260 continental silicate mineral assemblage (GEOCLIM-REG) maintains the steady-state $p\text{CO}_2$ below the
261 threshold for initiation of continental ice sheets but above unreasonably low values (<200 ppm). However,
262 as the reviewer points out, there are uncertainties in the modeling. For example, if the solid Earth
263 degassing rates increased through the Pennsylvanian (we invoke a constant CO_2 degassing rate), then it
264 is feasible that an increased component of weathering of mafic rocks would have maintained sufficiently
265 high CO_2 concentrations to accommodate the independent evidence for surface conditions at this time.

266 To that end, we have tempered the statements in Lines 318 to 328 (**lines 340-350** after changes suggested
267 by reviewers 1 and 2) by revising the text as follows:

268 “If peak ophiolite exhumation and maximum CO_2 consumption by their weathering occurred in the late
269 Carboniferous, thus initiating the LPIA (~330 to 300 Ma) as has been suggested (Table S1 of Macdonald
270 et al., 2019), then our modeling results suggest that a substantial increase in solid Earth degassing rate at
271 this time would have been necessary. In our simulation, increasing the surface area of outcropping mafic
272 rocks (2- to 4-fold) during the Pennsylvanian results in steady-state atmospheric CO_2 levels approaching
273 Snowball Earth conditions given other operating influences on weatherability and CO_2 sequestration at
274 the time and no change in degassing rate (Fig. S6). Such conditions are not compatible with proxy inferred
275 moderate surface conditions of the late Carboniferous (Montañez and Poulsen, 2013) and the radiation of
276 forest ecosystems throughout the tropics (DiMichele, 2014). Rather, we hypothesize that the sustained
277 CO_2 nadir and expansion of ice sheets in the first 10 Myr of the Permian record a major reorganization of
278 the predominant factors influencing weatherability in the tropics across the Carboniferous-Permian
279 transition, in particular, a substantial shift in the ratio of mafic-to-granitic rocks available for weathering.”

280

281 **ADDITIONAL CHANGES MADE TO MANUSCRIPT.**

282 In addition to the changes referenced in the “Response to Anonymous Referee #1” and “Response to
283 Anonymous Referee #2” documents, we undertook the following additional changes:

284

- 285 1) Changed the in-text citations for consistency and clarity.
- 286 2) Made changes to text where necessary to improve consistency and clarity and to rectify
287 typographical errors.
- 288 3) Added a citation for “Chen, J., Chen, B., and Montañez, I.P., in press, Carboniferous isotope

289 stratigraphy. In S. Lucas, J.W. Schneider, X. Wang, and S. Nikolaeva (eds.), *The Carboniferous*
290 *Timescale: Geol. Soc., London, Special Publication.*” in order to reference the latest information
291 of carbon and strontium isotopes during the LPIA and its demise.

- 292 4) Rearranged references to conform with the rules stated on the Climate of the Past website
293 pertaining to ordering of references.

294
295 In addition to the changes made to the main text outlined above, similar changes were made to the
296 supplementary material for consistency and clarity.

297 **MARKED UP VERSION OF MANUSCRIPT:**

298
299 **Influence of temporally varying weatherability on CO₂–climate**
300 **coupling and ecosystem change in the late Paleozoic.**

301
302 Jon D. Richey^{1*}, Isabel P. Montañez^{1*}, Yves Goddérís², Cindy V. Looy³, Neil P. Griffis^{1,4}, William A.
303 DiMichele⁵

304
305 ¹Department of Earth and Planetary Sciences, University of California, Davis, Davis, CA 95616, USA.

306 ²Géosciences Environnement Toulouse, CNRS – Université Paul Sabatier, Toulouse, France.

307 ³Department of Integrative Biology and Museum of Paleontology, University of California, Berkeley, Berkeley, CA 94720,
308 USA.

309 ⁴Berkeley Geochronology Center, Berkeley, CA 94720, USA.

310 ⁵Department of Paleobiology, Smithsonian Museum of Natural History, Washington, DC 20560, USA.

311
312 *Correspondence to: Jon D. Richey (jdrichey@ucdavis.edu); Isabel P. Montañez (ipmontanez@ucdavis.edu)

313
314 **Abstract** Earth’s penultimate icehouse, the Late Paleozoic Ice Age (LPIA), was a time of dynamic glaciation and repeated
315 ecosystem perturbation, under conditions of substantial variability in atmospheric $p\text{CO}_2$ and O_2 . Improved constraints on the
316 evolution of atmospheric $p\text{CO}_2$ and $\text{O}_2:\text{CO}_2$ during the LPIA and its subsequent demise to permanent greenhouse conditions
317 is crucial for better understanding the nature of linkages between atmospheric composition, climate, and ecosystem
318 perturbation during this time. We present a new and age-recalibrated $p\text{CO}_2$ reconstruction for a 40-Myr interval (~313 to 273
319 Ma) of the late Paleozoic that (1) confirms a previously hypothesized strong CO_2 -glaciation linkage, (2) documents
320 synchronicity between major $p\text{CO}_2$ and $\text{O}_2:\text{CO}_2$ changes and compositional turnovers in terrestrial and marine ecosystems, (3)

321 lends support for a modeled progressive decrease in the CO₂ threshold for initiation of continental ice sheets during the LPIA,
322 and (4) indicates a likely role of CO₂ and O₂:CO₂ thresholds in floral ecologic turnovers. Modeling of the relative role of CO₂
323 sinks and sources, active during the LPIA and its demise, on steady-state *p*CO₂ using an intermediate complexity climate-C
324 cycle model (GEOCLIM) and comparison to the new multi-proxy CO₂ record provides new insight into the relative influences
325 of the uplift of the Central ~~Pangae~~Pangean Mountains, intensifying aridification, and increasing mafic rock to-granite rock
326 ratio of outcropping rocks on the global efficiency of CO₂ consumption and secular change in steady-state *p*CO₂ through the
327 late Paleozoic.

328

329 **1 Introduction**

330 Earth's penultimate and longest-lived icehouse (340 to 290 Ma) occurred under the lowest atmospheric CO₂ concentrations of
331 the last half-billion years (Foster et al., 2017) and, potentially, the highest atmospheric *p*O₂ of the Phanerozoic (Glasspool et
332 al., 2015; Krause et al., 2018; Lenton et al., 2018). Anomalous atmospheric composition, along with 3% lower solar luminosity
333 (Crowley and Baum, 1992), may have primed the planet for a near-miss global glaciation (Feulner, 2017). Notably, Earth's
334 earliest tropical forests assembled and expanded during this icehouse (the Late Paleozoic Ice Age; LPIA), leading to the
335 emergence of large-scale wildfire. Paleotropical terrestrial ecosystems underwent repeated turnovers in composition and
336 architecture, culminating in the collapse of wetland (coal) forests throughout tropical Pangea at the close of the Carboniferous
337 (Clea and Thomas, 2005; DiMichele, ~~2014~~2014), possibly promoting the diversification and ultimate dominance of amniotes
338 (Pardo et al., 2019). In the marine realm, global rates of macroevolution (origination, extinction) decreased, in particular among
339 tropical marine invertebrates, and genera with narrow latitudinal ranges went extinct at the onset of the LPIA (Stanley, 2016;
340 Balseiro and Powell, 2019). Low marine macroevolutionary rates continued through to the demise of the LPIA in the early
341 Permian (Stanley and Powell, 2003; McGhee, 2018).

342 Reconstructions of late Paleozoic atmospheric *p*CO₂ document a broad synchronicity between shifts in CO₂, glaciation
343 history, glacioeustasy, and restructuring of paleotropical biomes, underpinning the hypothesized greenhouse-gas forcing of
344 sub-million-year glacial-interglacial cycles (Montañez et al., 2016) and the terminal demise of the LPIA (Montañez et al.,
345 2007). For late Paleozoic *p*CO₂ (and *p*O₂) reconstructions, however, broad intervals of low temporal resolution and significant

346 uncertainties limit the degree to which mechanistic linkages between atmospheric composition, climate, and ecosystem change
347 can be further evaluated. Moreover, the potential impact of large magnitude fluctuations in atmospheric O₂:CO₂, which
348 characterized the late Paleozoic, on the biosphere has been minimally addressed. On longer timescales ($\geq 10^6$ yr), the relative
349 role of potential CO₂ sinks and sources on secular changes in late Paleozoic atmospheric CO₂ and, in turn, as drivers of
350 glaciation and its demise, remain debated (McKenzie et al., 2016; Godd ris et al., 2017; Macdonald et al., 2019).

351 Here, we present a multi-proxy atmospheric *p*CO₂ reconstruction for a 40-Myr interval (313 to 273 Ma) of the late
352 Paleozoic, developed using new leaf fossil-based estimates integrated with recently published and age-recalibrated
353 Pennsylvanian *p*CO₂ estimates of 10⁵-yr resolution (Monta ez et al., 2016), and re-evaluated fossil soil- (paleosol) based CO₂
354 estimates for the early Permian (Monta ez et al., 2007). Our new multi-proxy record offers higher temporal resolution than
355 existing archives while minimizing and integrating both temporal and CO₂ uncertainties. This *p*CO₂ reconstruction, together
356 with new O₂:CO₂ estimates of similar temporal resolution, permits refined interrogation of the potential links between
357 fluctuations in atmospheric composition, climate shifts, and ecosystem events through Earth's penultimate icehouse.
358 Moreover, comparison of the new 40-Myr CO₂ record with modeled steady-state *p*CO₂ and seawater ⁸⁷Sr/⁸⁶Sr over the same
359 interval provides new insight into the relative importance and evolution of CO₂ sinks and sources during late Paleozoic
360 glaciation and its turnover to a permanent greenhouse state.

361

362 **2 Materials and Methods**

363 A brief account of the methods is presented here; more details are presented in the Supplementary Materials and Methods.
364 Primary data generated or used in this study [is/are](#) deposited in the Dryad Digital Repository (Richey et al., 2020) and can be
365 accessed at <https://doi.org/10.25338/B8S90Q>.

366

367 **2.1 Sample Collection and Analysis**

368 To build the *p*CO₂ record, 15 plant cuticle fossil species/morphotypes were used, collected from eight localities in Illinois,
369 Indiana, Kansas, and Texas, [U.S.A., USA](#), including four well-studied Pennsylvanian interglacial floras (Sub-Minshall [313
370 Ma;  im nek, (2018) [\],](#) Kinney Brick [305.7 Ma; DiMichele et al., (2013) [\],](#) Lake Sarah Limestone [303.7 Ma;  im nek,

371 ~~(2018)~~ and Hamilton Quarry [302.7 Ma; Hernandez-Castillo et al., ~~(2009a, b, c)~~; Figs. 1a, S2–4, Richey et al., ~~(2020)~~,
372 <https://doi.org/10.25338/B8S90Q>). The Pennsylvanian estimates were integrated into a previously published $p\text{CO}_2$
373 reconstruction (313 to 296 Ma; Montañez et al., ~~(2016)~~) of 10^5 -yr resolution built using pedogenic carbonates and wet-adapted
374 seed fern fossils (Figs. 2b, S1b). The Permian estimates were integrated with previously published latest Carboniferous and
375 early Permian pedogenic carbonate-based CO_2 estimates (Montañez et al., 2007), derived from paleosols from successions
376 throughout Arizona, New Mexico, Oklahoma, Texas, and Utah, ~~U.S.A-USA~~ (Fig. 1a, Richey et al., ~~(2020)~~,
377 <https://doi.org/10.25338/B8S90Q>). The pedogenic carbonates and leaf ~~fossil-cuticle~~ cuticle fossils span a broad region of
378 Pennsylvanian and early Permian tropical Euramerica (Figs. 1b). Ages of samples used in Montañez et al., (2007) and (2016)
379 were recalibrated and assigned uncertainties using the latest geologic timescale (Ogg et al., 2016) and biostratigraphic and
380 geochronologic controls (see Supplementary Materials and Methods; Richey et al., ~~(2020)~~, 2020,
381 <https://doi.org/10.25338/B8S90Q>).

382 Cuticle and organic matter occluded within pedogenic carbonates (OOM) were rinsed or dissolved, respectively, in 3M
383 HCl to remove carbonates and analyzed at the Stable Isotope Facility, University of California, Davis, using a PDZ Europa
384 ANCA-GSL elemental analyzer interfaced to a PDZ Europa 20-20 IRMS. External precision, based on repeated analysis of
385 standards and replicates, is $\leq \pm 0.2\%$. For Hamilton Quarry (HQ), all material was previously mounted on slides for taxonomic
386 analysis (Hernandez-Castillo et al., 2009a; Hernandez-Castillo et al., 2009b, c). Because of this, biomarker $\delta^{13}\text{C}$ values of bulk
387 stratigraphic sediment samples were used (Richey et al., unpublished data; see Supplementary Materials and Methods). HQ n -
388 C_{27-31} n -alkane $\delta^{13}\text{C}$ was analyzed using a Thermo Scientific GC-Isolink connected to a Thermo Scientific MAT 253. Standard
389 deviation of n -alkane $\delta^{13}\text{C}$ was $\pm 0.3\%$. For biomarker $\delta^{13}\text{C}$, a +4‰ correction was used to account for fractionation during
390 biosynthesis (Diefendorf et al., 2015) and the standard deviation of all values was used as the uncertainty (1.6‰, five times
391 the analytical precision).

393 2.2 Models

394 The MATLAB model Paleosol Barometer Uncertainty Quantification (PBUQ; Breecker, ~~(2013)~~, which fully propagates
395 uncertainty in all input parameters, was used to derive pedogenic carbonate-based CO_2 estimates (Figs. 2a, S1a). For each

396 locality, paleosols of inferred different soil orders were modeled separately. We applied improved soil-specific values for soil-
397 respired CO₂ concentrations ($S_{(z)}$; [Montañez et al., 2013](#)) and the $\delta^{13}\text{C}$ of organic matter occluded within carbonate nodules
398 ($\delta^{13}\text{C}_{\text{OOM}}$; Fig. S5) as a proxy of soil-respired CO₂ $\delta^{13}\text{C}$. For samples where OOM was not recovered, estimates were revised
399 using PBUQ and the plant fossil organic matter $\delta^{13}\text{C}$ used in [Montañez et al., \(2007\)](#) ($\delta^{13}\text{C}_{\text{POM}}$; Fig. S5). Because of the limited
400 amount of carbonate nodules remaining after study by [Montañez et al., \(2007\)](#), $\delta^{13}\text{C}_{\text{OOM}}$ was substituted for $\delta^{13}\text{C}_{\text{POM}}$ for
401 localities that occur in the same geologic formation and a large error ($\pm 2\%$) was used to account for the uncertainty in this
402 approach. PBUQ model runs conducted in this study resulted in a small subpopulation of biologically untenable CO₂ estimates
403 (i.e., ≤ 170 ppm; [Gerhart and Ward, \(2010\)](#)). To limit estimates below that threshold, two changes to the PBUQ Matlab code
404 were made (see Supplementary Materials and Methods for details). All other input parameters remained unchanged from
405 [Montañez et al., \(2007\)](#).

406 For cuticle fossil-based (Figs. S2–4) CO₂ estimates (Fig. 2a, S1a), we utilized a mechanistic (non-taxon-specific) gas-
407 exchange model ([Franks et al., 2014](#)). For some fossil cuticles, pore length (PL) was measured directly; for others, PL was
408 inferred from guard cell length (GCL; Table S2). Guard cell width was estimated via GCL using the prescribed gymnosperms
409 and ferns scaler (0.6; [Franks et al., \(2014\)](#); Table S2).

410 For both stomatal and pedogenic-carbonate-based CO₂ modeling, we calculated $\delta^{13}\text{C}$ of atmospheric CO₂ using the
411 carbonate $\delta^{13}\text{C}$ record generated from an open-water carbonate slope succession ([Naqing succession, South China; Buggisch](#)
412 [et al., \(2011\)](#)), contemporaneous estimates of mean annual temperature ([Tabor and Montañez 2005; Tabor et al., 2013](#)), and
413 temperature-sensitive fractionation between low-Mg calcite and atmospheric CO₂ ([Romanek et al., \(1992\)](#); Eq. S2; Table S2).

414 We used the spatially resolved, intermediate complexity GEOCLIM model ([Goddéris et al., 2014](#)) to quantitatively
415 evaluate how steady-state atmospheric CO₂ may have responded to changes in weatherability and relative influence of different
416 CO₂ sources and sinks. The spatial distributions of the mean annual runoff and surface temperature were calculated offline for
417 five time increments ([Goddéris et al., 2017](#)) covering the period of interest and for various atmospheric CO₂ levels using the
418 3D ocean-atmosphere climate model FOAM [\(and the approach as described in Donnadiu et al., 2016\(2006\)\)](#). GEOCLIM uses
419 generated lookup tables to calculate steady-state atmospheric CO₂ for a given continental configuration and to account for
420 paleogeography and relief. Although GEOCLIM model does not include an explicit surface distribution of lithology,

421 weathering rate of mafic rocks and continental granites are calculated using different methods and the impact of physical
422 erosion on granite weathering is accounted for (Goddéris et al., 2017). For mafic surfaces, a simple parametric law is used,
423 linking the surface of the considered grid cell, the local runoff, and mean annual temperature to the local mafic weathering
424 rate. The calibration of the GEOCLIM model was performed at the continental-scale by tuning the parameters of the model so
425 that 30% of the alkalinity generated by the weathering of silicates originates from the weathering of mafic rocks
426 (GEOCLIM_REG; Dessert et al., 2001; Goddéris et al., 2014).

427

428 **2.3 O₂:CO₂**

429 O₂:CO₂ ratios (Fig. 3a) were calculated using the 10,000 CO₂ estimates produced by our modeling and combined with O₂
430 estimates obtained using geochemical mass balance and biogeochemical models (Krause et al., 2018; Lenton et al., 2018).
431 Unreasonably high O₂:CO₂ (generally those that correspond to CO₂ ~<200 ppm) were removed from the resulting 10,000
432 O₂:CO₂ data set.

433

434 **2.4 Statistical Analyses**

435 We utilize a bootstrap approach that assesses uncertainties of both CO₂ (or O₂:CO₂) and age. Each age uncertainty was
436 truncated to ensure no overlap in locality ages, constrained by their relative stratigraphic position to one another (Richey et al.,
437 2020); <https://doi.org/10.25338/B8S90Q>). The 10,000 modeled CO₂ estimates were trimmed by 28% to remove anomalously
438 high/low values. The means of the resulting 7,200 CO₂ estimates were compared to the trimmed means of the 10,000 CO₂
439 estimates to ensure that trimming did not alter the central tendency of the data. Locality ages were resampled and perturbed,
440 assuming that the individual ages and truncated age uncertainties represent the mean and standard deviation of the ages.
441 Similarly, the trimmed CO₂/O₂:CO₂ datasets were resampled and the resampled ages and estimates were used to build 1000
442 resampled datasets. Each resampled dataset was subjected to LOESS analysis (0.25 smoothing) and the median and 95% and
443 75% confidence intervals were calculated (Figs. 2, 3a–b, S1). The Pennsylvanian and Permian portions of the record were
444 analyzed separately due to differing data density, with significant overlap across the Pennsylvanian-Permian boundary interval
445 (Figs. 2b, 3b, S1b).

Formatted: Indent: First line: 0"

446 To test the validity of short-term fluctuations in the LOESS CO₂ trend, we undertook further analysis of the raw Monte
447 Carlo data produced by PBUQ and the mechanistic stomatal model in several short-term increments, ~~by calculating individual~~
448 ~~CO₂ data points via bootstrapping for each increment (Figs. 2b, S1b).~~ Eleven short-term highs or lows (A–K on Fig. 4A) were
449 designated and used to form bins of ±0.5 to ±1 Myr. Within an individual bin, each shown ‘bootstrapped’ CO₂ data point is
450 the trimmed mean of 10,000 Monte Carlo model runs. The Monte Carlo model runs for each data point were sorted from
451 lowest to highest CO₂ value and the lowest CO₂ values for each data point within the bin were averaged. This averaging was
452 repeated sequentially for each of the 10,000 values creating 10,000 means for each bin (n=11). To evaluate whether a visually
453 perceived rise or fall (e.g., A to B decrease or B and C increase) is statistically valid, the 10,000 means of two adjacent bins
454 were compared sequentially with one another (i.e., the mean of the lowest values of one bin was compared to the mean of the
455 lowest values of the adjacent bin) in order to calculate a percent change $((V_2 - V_1)/V_1) * 100$ for each of the 10,000 model
456 runs, resulting in 10,000 percent changes for each set of adjacent bins. The percent of the 10,000 comparisons that confirm an
457 increase or decrease between bins is reported (Fig. 4B–J) as a measure of the statistical significance of the short-term
458 fluctuations in CO₂ concentration visually observed on the LOESS trend.

459

460 3 Results

461 Revised early Permian mineral-based CO₂ estimates define a substantially narrower range (45–1150 ppm; Fig. 2a) than
462 previous estimates (175–3500 ppm) made using the same pedogenic carbonate sample set (Montañez et al., 2007) while
463 maintaining the original trends and including fewer photosynthetically untenable concentrations (≤170 ppm; Gerhart and
464 Ward, (2010)). New early Permian cuticle-based estimates show a high level of congruence by locality and broad plant
465 functional type, falling within the revised pedogenic-based CO₂ range (Figs. 2a, S1a). Similarly, stomatal-based estimates for
466 the four Pennsylvanian interglacial floras are within the estimated pCO₂ range defined by the pedogenic carbonates (Fig. 2a,
467 S1a) and late-glacial wetland plant fossils (Montañez et al., 2016). ~~Notably, the newly integrated record confirms that elevated~~
468 ~~atmospheric CO₂ concentrations (482 to 713 ppm [-28/+72 ppm]) during Pennsylvanian interglacials (10⁴-yr) were elevated~~
469 ~~(482 to 713 ppm [-28/+72 ppm]) relative to in comparison to pCO₂ during glacial periods (161 to 299 ppm [-96/+269 ppm]);),~~
470 ~~with interglacial durations on the order of 1000s to 10s of 1000s of years given the inferred eccentricity scale duration of the~~

Formatted: Default Paragraph Font, English (United Kingdom)

Formatted: Default Paragraph Font, English (United Kingdom)

Formatted: Default Paragraph Font, English (United Kingdom), Not Superscript/ Subscript

Formatted: Default Paragraph Font, English (United Kingdom)

Formatted: Default Paragraph Font, English (United Kingdom)

Formatted: Default Paragraph Font, English (United Kingdom)

471 [glacial-interglacial cycles \(Horton et al. 2012; Montañez et al. 2016; Fielding et al. 2020\)](#),

472 Overall, the new $p\text{CO}_2$ record documents declining CO_2 through the final 13-Myr of the Pennsylvanian into the earliest
473 Permian, including a 2.5-Myr interval (307 ~~and~~to 304.5 Ma) of minimum CO_2 values (~~less than~~ 400 to ~~as low as~~ 200 ppm)
474 in the Kasimovian (Fig. 2b, S1b). Declining $p\text{CO}_2$ in the late Carboniferous coincides with rising atmospheric $p\text{O}_2$ (Glasspool
475 et al., 2015; Krause et al., 2018; Lenton et al., 2018); thus, $\text{O}_2\text{:CO}_2$ ratios in the interval of minimum Pennsylvanian CO_2 are
476 nearly two times those of present-day (~515; gray line in Fig. 3a). A 10-Myr CO_2 nadir (~180 to <400 ppm) characterizes the
477 first two stages (Asselian and Sakmarian; 298.9 to 290.1 Ma) of the early Permian, overlaps with the peak occurrence of glacial
478 deposits in the LPIA (gray boxes in Fig. 2b; Soreghan et al., (2019)), and defines a second interval of anomalously high
479 $\text{O}_2\text{:CO}_2$ ratios (up to 970 ppm; Fig. 3a). A subsequent long-term rise (~17 Myr) in $p\text{CO}_2$ to peak values up to ~740 ppm (-
480 190/+258 ppm) defines the remainder of the early Permian and coincides with multiple episodes of extensive and long-lived
481 volcanism (Fig. 2b; Torsvik et al., (2008); Zhai et al., (2013); Sato et al. (2015); Shellnutt, (2018); Chen and Xu, (2019)).
482 This $p\text{CO}_2$ rise is also coincident with a decline in $\text{O}_2\text{:CO}_2$ to below present-day values (Fig. 2b, S1b, 3a).

483 Short-term intervals of rising or falling CO_2 in the LOESS trend, within dating uncertainties, coincide with a brief but
484 acute glaciation in the Kasimovian and with repeated deglaciations in south-central Gondwana in the early Permian (Griffis et
485 al., 2018; Griffis et al., 2019), as well as with restructuring of marine and terrestrial ecosystems (Figs. 3b-d). The statistical
486 significance of these short-term rises and falls in CO_2 was evaluated by analyzing the raw Monte Carlo estimates (10,000
487 model runs per data point shown on the LOESS trend) generated by the aforementioned CO_2 models (Breecker, 2013; Franks
488 et al., 2014), from which the bootstrapped CO_2 estimates for eleven increments of short-term rise or fall were subsequently
489 determined (Fig. 4a). The analysis of the Monte Carlo CO_2 estimates within these short-term intervals of rising or falling CO_2
490 indicates that 72.5 to 100% of the data confirm a visually observed increasing or decreasing trend (Fig. 4).

491 **4 Discussion**

492 **4.1 Declining CO_2 through the Main Phase of the LPIA**

493 Atmospheric CO_2 concentrations in the final 13 Myr of the Carboniferous (the Pennsylvanian portion of our record) are
494 generally higher than those of the earliest Permian (Fig. 2b) and overall decline through the later part of the Carboniferous.
495

Formatted: Default Paragraph Font, English (United Kingdom)

Formatted: Subscript

496 Higher $p\text{CO}_2$ in the latter half of the Pennsylvanian is compatible with the hypothesized waning of large Early to Middle
497 Pennsylvanian glaciers in the Late Pennsylvanian (c.f. Fielding et al., (2008), including widespread terminal deglaciation in a
498 major glacial depocenter in south-central Gondwana (Parana Basin, Brazil) toward the close of the Carboniferous (Griffis et
499 al., 2018; Griffis et al., 2019). Declining $p\text{CO}_2$ toward a nadir in the earliest Permian is also consistent with a renewed increase
500 in the geographic distribution of glacial deposits in Gondwana beginning in the Late Pennsylvanian and peaking (~~apex~~) in the
501 earliest Permian (Fig. 2b; Soreghan et al., (2019)).

502 A tectonically driven increase in CO_2 consumption via a strengthening of the silicate weathering ('climate stabilizing')
503 negative feedback (Walker et al., 1981; Berner and Caldeira, 1997) has been proposed as the driver of the Pennsylvanian
504 decline in $p\text{CO}_2$ (Godd ris et al., 2017). The strength of the negative feedback varies with the degree of 'weatherability' (i.e.,
505 the susceptibility to weathering), which, in turn, is predominantly controlled by the intensity of the hydrologic cycle
506 (precipitation and surface runoff), with further influence by surface temperature and vascular plants (Dessert et al., 2001;
507 Donnadi u et al., 2004; West, 2012; Maher and Chamberlain, 2014; Caves et al., 2016; Ibarra et al., 2016). Uplift of the Central
508 ~~Pangaeaan~~Pangean Mountains (CPM) through the Pennsylvanian would have increased weatherability in the tropics by inducing
509 orographic precipitation and creating steeper slopes (Godd ris et al., 2017), thus providing a greater supply of fresh mineral
510 surfaces and enhanced surface runoff ~~and with longer~~ fluid travel paths (cf. Maher and Chamberlain, 2014). Consequently,
511 CPM-induced increased weatherability and CO_2 consumption would have enhanced the global efficiency of weathering and
512 created a tighter coupling between CO_2 and climate at this time (cf. Maher and Chamberlain, (2014); Caves et al., (2016)).

513 The results of our GEOCLIM modeling, for a Himalayan-type mountain range (an analog for the CPM) and
514 parameterized such that 30% of the alkalinity generated by silicate weathering originates from the weathering of mafic rocks
515 (referred to as the 'reference continental silicate mineral assemblage or GEOCLIM_REG), indicates steady-state CO_2
516 concentrations (blue symbols and lines on Fig. 5A and B) that are well below the middle to late Carboniferous (340 to 300
517 Ma) threshold for initiation of continental ice sheets (840 ppm; Lowry et al., (2014). A hypothesized primary influence of the
518 CPM on CO_2 consumption through increased weatherability is further supported by the coincidence of modeled seawater and
519 marine proxy $^{87}\text{Sr}/^{86}\text{Sr}$ values that define a plateau of peak radiogenic values that is sustained for 15-Myr of the late
520 Carboniferous (318 to 303 Ma; Fig. 5b). The proxy-based seawater $^{87}\text{Sr}/^{86}\text{Sr}$ plateau has been long interpreted to record

Formatted: Default Paragraph Font, English (United Kingdom)

521 exposure and weathering of uplifted and metamorphosed crustal rocks of the CPM that had radiogenic Sr isotope compositions
522 (Chen et al., (2018) and references within).
523 ; Chen et al., in press). Additionally, the burial of substantial organic matter as peat in swamp environments prone to
524 preservation (ultimately as coal) during the Pennsylvanian would have partitioned global CO₂ consumption between silicate
525 weathering and organic carbon burial, further driving a lower steady-state pCO₂ lower (D'Antonio et al., 2019; Ibarra et al.,
526 2019). Our modeling, however, assumes a constant pre-Hercynian solid Earth degassing through the study interval and does
527 not account for increased magmatic CO₂ during Hercynian arc-continent collision and potential widespread eruptive volcanism
528 in the late Carboniferous (Soreghan et al., 2019), both of which could have increased steady-state CO₂.

529 Short-term fluctuations in pCO₂ are superimposed on the 40-Myr record and long-term decline through the latter portion
530 of the Carboniferous. These short-term fluctuations have been confirmed as statistically significant (99.9 to 100% of estimates;
531 Fig. 4b-d) and coincide with major environmental and biotic events. The brief interval of minimum pCO₂ (an average of
532 ~300 ppm, but as low as 180 ppm) in the late Carboniferous (Kasimovian Stage, 307 to 304.5 Ma; Fig. 3b) coincides with a
533 short-lived but acute glaciation (306.5 to 305 Ma) recorded by prominent valley incision and large-scale regression recorded
534 by cyclothemic successions in the U.S.-US Appalachian Basin and Midcontinent, as well as the Donets Basin, Ukraine (Belt et
535 al., 2011; Eros et al., 2012; Montañez et al., 2016). Significant and repeated restructuring of wetland forests throughout tropical
536 Euramerica, involving quantitative changes in floral composition and dominance, occurred during this 2.5 Myr pCO₂ minimum
537 (and O₂:CO₂ maximum; Fig. 3a-c). Before the short-term pCO₂ low, Euramerican tropical forests had expanded to their
538 maximum aerial extent ($\geq 2 \times 10^6$ km²) under CO₂ concentrations of ~500 ppm (Moscovian Stage, Fig. 3b). The aerial extent
539 of these forests dropped by half (green X in Fig. 3c; Cleal and Thomas, (2005)) coincident with the decline in pCO₂ and near
540 doubling of O₂:CO₂ (Fig. 3a-b). Moreover, within this pCO₂ low (Fig. 3b), arborescent lycopsids of the wetland forests went
541 extinct throughout Euramerica (white X in Fig. 3c) and seasonally dry tropical floras shifted from cordaitalean- to walchian-
542 dominance (~307–306.8 Ma; Fig. 3c; DiMichele et al., (2009); Falcon-Lang et al., (2018)). These restructuring events
543 occurred at or proximal to CO₂ falling below 400 ppm, supporting a previously hypothesized but untested CO₂ threshold for
544 the Pennsylvanian ecologic turnovers (Fig. 3b-c; Beerling et al., (1998); Beerling and Berner, (2000); Montañez et al., (2016).
545 In the oceans, foraminiferal diversity decreased substantially during the Kasimovian pCO₂ low with the loss of ~200 species

546 (~58% of all taxa; ~~1st~~ first gray bar in Fig. 3d; Groves and Yue, (2009)) presumably due to decreasing seawater temperatures.

547 The interval of CO₂ minima was terminated by a rapid rise across the Kasimovian-Gzhelian boundary (303.7 Ma) to CO₂
548 concentrations above 600 ppm (Fig. 2b; S1b). The short-term interval of elevated pCO₂ (304 to 302.5 Ma) is coincident with
549 a ~1.5‰ decline in seawater δ¹³C (Grossman et al., 2008; Chen et al., in press), compatible with a decline in the CO₂ sink
550 provided by terrestrial organic C (peats) burial (gray bar on Fig. 2b) and/or a peak in pyroclastic volcanism between ~310 and
551 301 Ma (Soreghan et al., 2019). This period of increased pCO₂ overlaps with the Alykaevo Climatic Optimum (orange bar on
552 Fig. 3c), defined by the invasion of tropical Euramerican vegetation into the *Rufloia*-dominated, mid-latitude Angaran floral
553 province (Cleal and Thomas, 2005). Terminal deglaciation in south-central Gondwana (Parana Basin, Brazil), U-Pb dated to
554 between ~302 and 298 Ma (Cagliari et al., 2016; Griffis et al., 2018), may have been linked to the Late Pennsylvanian interval
555 of elevated CO₂, although this requires further testing (Figs. 2b, 3b). Conversely to the Kasimovian CO₂ low, a significant
556 change in global diversity of foraminifera involving a doubling of species occurred during this subsequent period of elevated
557 CO₂ and presumed increase in seawater temperatures (black bar on Fig. 3d; Groves and Yue, (2009)).

558 559 4.2 An Early Permian CO₂ Nadir

560 Atmospheric pCO₂ dropped substantially across the Carboniferous-Permian Boundary (i.e., 298.9 Ma) to a 10-Myr interval
561 (300–290 Ma) of the lowest concentrations (~~160~~175 to <400 ppm) of the 40-Myr record (Fig. 2b). The CO₂ nadir, which spans
562 the Asselian and Sakmarian stages, coincides with renewed glaciation and maximum ice sheet extent, marking the apex of
563 LPIA glaciation (Fig. 2b; Fielding et al., (2008); Isbell et al., (2012); Montañez and Poulsen, (2013); Soreghan et al.,
564 (2019)), as well as with a large magnitude eustatic fall archived in paleotropical successions worldwide (Koch and Frank,
565 2011; Eros et al., 2012). Widespread glacial expansion temporally linked to this interval of lowest overall pCO₂ argues for
566 CO₂ as the primary driver of glaciation rather than recently proposed mechanisms, such as the influence of the closing of the
567 Precaspian Isthmus (Davydov, 2018) or a decrease in the radiative forcing resulting from increased atmospheric aerosols by
568 explosion volcanism at this time (Soreghan et al., 2019). The very low greenhouse radiative forcing associated with this low
569 CO₂ interval would have been amplified by 2.5% lower solar luminosity (Crowley and Baum, 1992), reduced transmission of
570 short-wave radiation (Poulsen et al., 2015) by the high pO₂ atmosphere of the early Permian (Krause et al., 2018; Lenton et
571 al., 2018), and by increased atmospheric aerosols at this time (Soreghan et al., 2019).

Formatted: Font: Not Bold

572 ~~Notably, the~~The 10-Myr $p\text{CO}_2$ nadir raises a paradox as to what was the primary CO_2 sink(s) at the time given that the
573 CO_2 sinks of the Pennsylvanian were no longer prevalent. This paradox reflects the waning denudation rates of the CPM by
574 the early Permian (Godd ris et al., 2017), intensifying pantropical aridification, possibly driven by increasing continentality
575 (yellow to red bar in Fig. 3c; DiMichele et al., (2009)); Tabor et al., (2013)); and the demise of the wetland tropical forests
576 and associated loss of peats before the close of the Carboniferous (black-to-gray bar in Fig. 2b; Hibbett et al., (2016)). In
577 turn, surface runoff would have been inhibited and the supply of fresh silicate minerals ~~dampened~~decreased, thus lowering
578 overall weatherability. Atmospheric CO_2 under the influence of these ~~aforementioned~~ environmental factors should have
579 equilibrated in the earliest Permian at a new higher steady-state level, even if solid Earth degassing did not increase (cf. Gibbs
580 et al., (1999)), thus raising a paradox. If volcanism was increasing by this time (Fig. 2b and associated references; Soreghan
581 et al., 2019), then this paradox is even greater.

582 The paradox, however, can be resolved if a switch in the ratio of mafic to granite rocks available for weathering occurred
583 with the turnover from the Carboniferous to the early Permian, in particular in the warm tropics. Two mechanisms have the
584 potential to resolve this paradox. The first, referred to as a delayed climate-controlled capacitor (Joshi et al. 2019), leads to a
585 multi-million-year delay between the timing of peak orogenic uplift and maximum chemical weathering potential and CO_2
586 drawdown due to substantial differences in chemical weathering rates during the different phases of an orogenic cycle. In their
587 study, the highest intensity of chemical weathering and capacity for CO_2 consumption occurs when mountains have been
588 somewhat denuded rather than during peak uplift, reflecting the disproportionate influence of runoff temperature over
589 hydrology and erosion on weathering potential. Notably, Joshi et al.'s (2019) coupled climate and geochemical modeling of
590 the Late Paleozoic Ice Age yield an evolution of simulated $p\text{CO}_2$ over the period of uplift and denudation of the CPM that
591 corresponds both in absolute CO_2 concentrations and magnitude of change over this period (~320 to 290 Ma). That said, in
592 Joshi et al. (2019), the physical erosion parameter is not dependent on climate, but, rather, is defined by the prescribed altitude.
593 Thus, physical erosion is an external forcing in their model. The absence of runoff dependence for physical erosion (as is the
594 case for GEOCLIM) and the strong dependence of weathering on temperature may be the trigger for their simulated delay
595 between maximum uplift and the highest intensity of CO_2 consumption by silicate weathering. In GEOCLIM, the dependence
596 of the physical erosion on runoff does not allow for millions of years delay between maximum uplift of the CPM and lowest

597 simulated pCO₂. Further study is needed to interrogate the influence of this approach on the results.

598 The second mechanism proposed here is a substantial shift in the ratio of mafic-to-granite rocks available for weathering
599 from the latest Carboniferous to the early Permian. This reflects the doubling or greater increase in weatherability of mafic
600 mineral assemblages over granitic assemblages (Gaillardet et al., 1999; Dessert et al., 2003; Ibarra et al., 2016), thus enhancing
601 weathering efficiency and CO₂ drawdowns, and creating a tighter coupling between CO₂ and climate. In turn, with
602 tighter coupling between CO₂ and climate, the global silicate weathering flux needed to maintain homeostatic balance in the
603 carbon cycle for a given scenario can be maintained/attained at a lower pCO₂ level.

604 Macdonald and others (2019) hypothesized that increased weatherability provided by the exhumation of ophiolites along
605 the ~10,000 km long Hercynian arc-continent suture zone, mainly/primarily situated in the paleotropics, was capable of
606 lowering pCO₂ below the ice initiation threshold in the Carboniferous (i.e., Pennsylvanian), thus instigating the Late Paleozoic
607 Ice Age. We Here, we used the GEOCLIM model to, first, interrogate this Carboniferous hypothesis further and, second, to
608 evaluate the potential of increased weatherability, provided by increasing the ratio of outcropping mafic rocks to granite rocks
609 available for weathering, as the predominant driver of the early Permian CO₂ nadir. Figure 5 illustrates the influence of a
610 successive increase in the surface area of outcropping mafic rocks beginning with the reference continental silicate mineral
611 assemblage (GEOCLIM-REG), which was used to evaluate the influence of Pennsylvanian uplift of the CPM, to an up to 4-
612 fold increase in the outcropping of mafic rocks. In the GEOCLIM context, the weathering of mafic rocks is dependent on the
613 surface of each grid cell, and of on the associated local runoff and air temperature, multiplied by a calibration constant.
614 Increasing the exposure area of mafic rocks is mathematically equivalent to multiplying the calibration constant.

615 Between 300 and 290 Ma, when predominant Pennsylvanian CO₂ sinks were lost (terrestrial organic C burial) or waning
616 (decreased precipitation and denudation rates of the CPM), modeled steady-state atmospheric CO₂ is maintained at or below
617 the CO₂ threshold for initiation of continental ice sheets (560 ppm; Lowry et al., (2014)) when the surface area of outcropping
618 mafic rocks is greater than 2-fold that of GEOCLIM-REG (Fig. 5a). Conversely, steady-state CO₂ rises well above the glacial
619 threshold (to 3500 pm) for the 'reference' continental silicate rock assemblage (Fig. 5a). Although volcanism remained
620 geographically extensive through the 10-Myr CO₂ nadir (Soreghan et al., 2019), the impact on atmospheric CO₂ would have
621 been short-lived (≤10⁵ kyr; Lee and Dee, (2019)), and eclipsed on the longer term by the increased weatherability provided

Formatted: Normal, Left, Border: Top: (No border), Bottom: (No border), Left: (No border), Right: (No border), Between : (No border), Bar : (No border)

Formatted: Default Paragraph Font

Formatted: Default Paragraph Font, Not Superscript/ Subscript

Formatted: Default Paragraph Font

Formatted: Default Paragraph Font, Not Superscript/ Subscript

Formatted: Default Paragraph Font

Formatted: Default Paragraph Font

Formatted: Default Paragraph Font

Formatted: Default Paragraph Font, Font: Not Italic

Formatted: Default Paragraph Font

Formatted: Default Paragraph Font, Not Superscript/ Subscript

Formatted: Default Paragraph Font

Formatted: Default Paragraph Font, English (United States), Border: : (No border), Text Outline

Formatted: Default Paragraph Font

Formatted: Default Paragraph Font

Formatted: Default Paragraph Font

Formatted: Default Paragraph Font

Formatted: Default Paragraph Font, Lowered by 2 pt

Formatted: Default Paragraph Font

622 by increased exposure of mafic rocks along the Hercynian arc-continent suture zone, lowering steady-state CO₂ to, potentially,
623 pre-volcanism levels (cf. Dessert et al., (2001)).

624 Independent evidence for a substantial shift in the partitioning of silicate weathering to more mafic mineral assemblages
625 in the earliest Permian exists in the late Paleozoic proxy-based seawater Sr isotope record, which documents a rapid
626 (0.000043/Myr) and near-linear decrease in seawater ⁸⁷Sr/⁸⁶Sr beginning in the latest Carboniferous (~303 Ma) and continuing
627 through into the middle Permian (Fig. 5b; Chen et al. (2018);, in press). The simulated trends in seawater ⁸⁷Sr/⁸⁶Sr for
628 GEOCLIM-REG (blue line on Fig. 5b) through a 2- to 4-fold increase in the area of exposed mafic rocks capture the rapid rise
629 through the upper Carboniferous to peak values in the latter half of the Pennsylvanian and subsequent decline through the early
630 Permian. The rapid rate of decline in proxy ⁸⁷Sr/⁸⁶Sr values post-300 Ma, however, is best bracketed by simulated ⁸⁷Sr/⁸⁶Sr for
631 a 2- to 4-fold increase in mafic rock exposure. Moreover, the best fit of the simulated trends to the geochronologically well-
632 constrained bioapatite data (blue and green crosses on Fig. 5b) suggests a progressive increase in mafic-to-granite ratio through
633 the 10-Myr CO₂ nadir. This finding, together with the hypothesized need (the aforementioned mechanism two) for minimally
634 a 4-fold increase in mafic-rock outcropping in order to maintain CO₂ concentrations below the ice initiation threshold for a
635 sustained period longer than that of hysteresis (i.e., throughout the interval of minimum CO₂ and apex of glaciation (Fig. 5),
636 argues for a substantial increase in weatherability from the Carboniferous to early Permian driven by a compositional shift in
637 outcropping rocks available for weathering to a higher mafic-to-granite ratio.

638 Although it has been suggested that if peak ophiolite exhumation and maximum CO₂ consumption by their weathering
639 occurred in the late Carboniferous, thus initiating the LPIA (~330 to 300 Ma; as has been suggested (Table S1 of Macdonald
640 et al., (2019)), then our modeling results indicate suggest that a substantial increase in solid Earth degassing rate at this is not
641 compatible with proxy-inferred moderate surface conditions of the late Carboniferous (Montañez and Poulsen, 2013) and the
642 radiation of forest ecosystems throughout the tropics (DiMichele, 2104). Increasing time would have been necessary. In our
643 simulation, increasing the surface area of outcropping mafic rocks (2- to 4-fold) during the Pennsylvanian results in steady-
644 state atmospheric CO₂ levels approaching Snowball Earth conditions given other operating influences on weatherability and
645 CO₂ sequestration at the time and no change in degassing rate (Fig. S6). For such Such conditions to be not compatible with
646 proxy inferred moderate surface conditions of the paleontological record requires invoking a substantial increase in solid Earth

Formatted: Default Paragraph Font

Formatted: Default Paragraph Font, Lowered by 2 pt

Formatted: Default Paragraph Font

Formatted: Corps, Justified

Formatted: Default Paragraph Font

Formatted: Default Paragraph Font

Formatted: Default Paragraph Font

Formatted: Default Paragraph Font

Formatted: Default Paragraph Font

Formatted: Default Paragraph Font

Formatted: Default Paragraph Font, Lowered by 2 pt

Formatted: Default Paragraph Font

Formatted: Default Paragraph Font, Lowered by 2 pt

Formatted: Default Paragraph Font

Formatted: Default Paragraph Font

Formatted: Default Paragraph Font

Formatted: Default Paragraph Font

Formatted: Default Paragraph Font

647 ~~degassing rates. Alternatively late Carboniferous (Montañez and Poulsen, 2013) and the radiation of forest ecosystems~~
648 ~~throughout the tropics (DiMichele, 2014). Rather,~~ we hypothesize that the sustained CO₂ nadir and expansion of ice sheets in
649 the first 10 Myr of the Permian record a major reorganization of the predominant factors influencing weatherability in the
650 tropics across the Carboniferous-Permian transition, in particular, a substantial shift in the ratio of mafic-to-granitic rocks
651 available for weathering.

652 Similar to the short-term fluctuations superimposed on the later Carboniferous long-term decline in CO₂, two statistically
653 significant (94 to 100% on Fig. 4e-h) short-term increases in pCO₂ are superimposed on the early Permian nadir (Fig. 3b). The
654 first (298 to 296 Ma) coincides, within age uncertainty, with a major deglaciation event in the Karoo (southern Africa) and
655 Kalahari (Namibia) basins of south-central Gondwana (296.41 Ma +0.27/-0.35 Ma; Griffis et al., 2019). The second short-
656 term rise in pCO₂ (294.5 to 292.5 Ma) overlaps with the onset of widespread ice loss in several southern Gondwanan ice centers
657 (Fig. 2b; Soreghan et al., 2019). This CO₂-deglaciation link suggests that continental ice stability in the early Permian dropped
658 substantially when pCO₂ rose above ~ 300 to 400 ppm and thus raises the question as to whether the ice sheet CO₂ threshold
659 was even lower than modeled (560 ppm; Lowry et al. 2014) during the earliest Permian.

661 4.3 Impact on Tropical Ecosystems

662 ~~The geologically rapid and large-magnitude drop in pCO₂ to a protracted~~Notably, the early Permian pCO₂ minimum (Fig. 6
663 2b, S1b) and ~~period of associated~~ anomalously high O₂:CO₂ (700 to 960; Fig. 3a) ~~would have impacted earliest Permian~~
664 ~~terrestrial ecosystems given that modeling studies indicate a decrease in photosynthetic rate and net primary productivity when~~
665 ~~plants are exposed to low (<400 ppm) CO₂ concentrations under elevated pO₂ (Beerling et al., 1998; Beerling and Berner,~~
666 ~~2000). Euramerican tropical forests underwent a permanent shift in plant dominance is an interval of major ecosystem changes.~~
667 The geologically rapid and large-magnitude drop in pCO₂ prior to and across the Carboniferous-Permian boundary interval
668 (Fig. 2b, S1b) coincides with a permanent shift in plant dominance from swamp-community floras to seasonally dry vegetation
669 (Black X on Fig. 3e);3c). That shift in plant dominance has been long attributed to intensification of an aridification trend that
670 began in the mid-Pennsylvanian (yellow to red bar in Fig. 3c; DiMichele et al., (2009); Tabor et al., (2013)). The high-water-
671 use efficiency (WUE) of the seasonally dry plants would have made them water stress-tolerant. Furthermore, and analogous)
672 Analogous to the vegetation turnover and extinction during the Pennsylvanian CO₂ minimum, this permanent shift in the

Formatted: Default Paragraph Font

Formatted: Default Paragraph Font, Not Superscript/
Subscript

Formatted: Default Paragraph Font

Formatted: Default Paragraph Font, Font: 10 pt

Formatted: Normal, Left, Indent: First line: 0.3", Border:
Top: (No border), Bottom: (No border), Left: (No border),
Right: (No border), Between : (No border), Bar : (No border)

Formatted: Default Paragraph Font

Formatted: Default Paragraph Font

Formatted: Default Paragraph Font, Not Superscript/
Subscript

Formatted: Default Paragraph Font

Formatted: Default Paragraph Font, Not Superscript/
Subscript

Formatted: Default Paragraph Font

Formatted: Default Paragraph Font

Formatted: Default Paragraph Font

Formatted: Default Paragraph Font

Formatted: Default Paragraph Font

Formatted: Default Paragraph Font

Formatted: Default Paragraph Font

Formatted: Default Paragraph Font

Formatted: Default Paragraph Font, Not Superscript/
Subscript

Formatted: Default Paragraph Font

Formatted: Default Paragraph Font

673 ~~tropics to~~ seasonally dry vegetation ~~is~~ coincident with the earliest Permian drop in $p\text{CO}_2$ to ~~concentrations~~ below 400 ppm
674 ~~suggests, suggesting~~ a possible ecophysiological advantage of these plants over the wetland floral dominants that they replaced
675 ~~(Fig. 3a–c; c.f., Wilson et al., (2017)). Moreover, this shift in vegetation dominance to)~~. The high water use efficiency of the
676 ~~seasonally dry~~ plants of ~~significantly higher WUE~~ would have made them water stress-tolerant and, in turn, would have
677 amplified ~~the~~ aridification through a modeled ~50% decrease in canopy-scale transpiration (Wilson et al., 2017; Wilson et al.,
678 2020). The extreme habitat restriction of wetland floras was particularly consequential for tetrapods, leading to the acquisition
679 of terrestrial adaptations in crown tetrapods and the radiation and eventual dominance of dryland-adapted amniotes, possibly,
680 shaping the phylogeny of modern terrestrial vertebrates (Fig. 3c; Pardo et al., (2019)).

681 ~~Notably~~Moreover, the CO_2 decline ~~aerossat~~ the Carboniferous-Permian boundary into the 10-Myr nadir and ~~early~~
682 ~~Permian~~associated peak in O_2/CO_2 also corresponds to the evolution and radiation of glossopterids and gigantopterids
683 (McLoughlin, 2011; Zhou et al., 2017), with increasing vein density in the former (Fig. 3a–c; Srivastava, (1991)). These plant
684 groups had complex, angiosperm-like venation (Melville, 1983; Srivastava, 1991), with gigantopterids having the only known
685 pre-Cretaceous vessels in their stems, ~~which would have increased their stem conductance of water~~ (Li et al., 1996).
686 ~~Increased~~The ~~increased~~ hydraulic capacity provided by these morphological characteristics would have conferred a significant
687 ecological advantage to these plants under the low CO_2 , high O_2 , and elevated aridity conditions in which they evolved (cf.
688 Gerhart and Ward, (2010); de Boer et al., (2016)). In the oceans, a marked collapse in foraminiferal diversity with a notable
689 fall in species to a minimum from a Pennsylvanian zenith (425 to 110 species; Fig. 3d, e; Groves and Yue, (2009)) spanned
690 the 10-Myr $p\text{CO}_2$ nadir, analogous to the diversity drop during the Pennsylvanian low CO_2 interval.

691 ~~Two statistically significant (94 to 100% on Fig. 4c–h), short-term increases in $p\text{CO}_2$ are superimposed on the early~~
692 ~~Permian nadir (Fig. 3b)). The first (298 to 296 Ma) coincides, within age uncertainty, with a major deglaciation event in the~~
693 ~~Karoo (southern Africa) and Kalahari (Namibia) basins of south-central Gondwana (296.41 Ma \pm 0.27/–0.35 Ma; Griffis et al.,~~
694 ~~(2019)). The second short-term rise in $p\text{CO}_2$ (294.5 to 292.5 Ma) overlaps with the onset of widespread ice loss in several~~
695 ~~southern Gondwanan ice centers (Fig. 2b; Soreghan et al., (2019)). This CO_2 deglaciation link suggests that continental ice~~
696 ~~stability in the early Permian dropped substantially when $p\text{CO}_2$ rose above 300 to 400 ppm and thus raises the question as to~~
697 ~~whether the ice sheet CO_2 threshold was even lower than modeled (560 ppm; Lowry et al. 2014) during the earliest Permian.~~

Formatted: Default Paragraph Font

Formatted: Default Paragraph Font

Formatted: Default Paragraph Font, Font: Not Italic

Formatted: Default Paragraph Font

Formatted: Default Paragraph Font, Not Superscript/ Subscript

Formatted: Default Paragraph Font

Formatted: Default Paragraph Font

Formatted: Default Paragraph Font

Formatted: Default Paragraph Font

Formatted: Default Paragraph Font

Formatted: Default Paragraph Font

Formatted: Default Paragraph Font

Formatted: Default Paragraph Font

Formatted: Font color: Black, Border: : (No border), Text Outline

Formatted: Default Paragraph Font

Formatted: Default Paragraph Font, Font color: Black, English (United States), Border: : (No border), Text Outline

4.4.3 CO₂-Forced Demise of the LPIA and Ecosystem Impact

The 10-Myr CO₂ nadir terminated at 290 Ma with the onset of a protracted CO₂ rise that persisted to the highest levels of the record (~740 ppm [-190/+258]) by the close of the early Permian (Fig. 2b). The onset of this protracted CO₂ rise overlaps with initiation of a period of large-magnitude magmatism (red bars in Fig. 2b). Widespread volcanism began around 297.4 Ma (\pm 3.8 Ma) in northern Europe (Skagerrak-centered Large Igneous Province), extending well into Germany (Rotliegend) (Torsvik et al., 2008; Käbner et al., 2019). The multi-stage Tarim magmatic episodes in China (292–272 Ma; with peaks at ~290 Ma and 280 Ma; Fig. 2b; Chen and Xu, (2019)), was likely associated with large magnitude CO₂ emissions given that the magma, which distributed basalt (400 m thick) over a 2.5×10^5 km² region (Yang et al., 2013), intruded a thick succession of early Paleozoic marine carbonates (Gao et al., 2017). The Panjal Traps, N-W-NW India (289 Ma \pm 3 Ma; (Shellnutt, 2018)) and the compositionally similar Qiangtang Dykes (283 Ma \pm 2 Ma; Fig. 2b; Zhai et al., (2013)), albeit relatively small in extent, were an additional potential volcanic CO₂ source, along with contemporaneous volcanism in Oman. Furthermore, protracted Choiyoi volcanism, which began at 286.5 Ma \pm 2.3 Ma (Sato et al., 2015) and continued over ~39 Myr in western Argentina, may have contributed substantial pulses of greenhouse gases in the early Permian (Spalletti and Limarino, 2017). Once each magmatic episode waned, however, the mafic-dominated magmatic deposits would have served as longer-term regional sinks leading to increased global CO₂ consumption (cf. Lee et al., (2015)). Thus, for steady-state CO₂ to have increased through the remainder of the early Permian, the relative influence of CO₂ inputs must have outpaced that of these, and other, outputs (CO₂ sinks).

Our modeled (GEOCLIM) steady-state CO₂ for a 4-fold increase in outcropping of mafic rocks surpasses the ice-sheet initiation threshold at the termination of the CO₂ nadir (~290 Ma; red line and symbols on Fig. 5a), despite no change in solid Earth degassing. That low CO₂ concentrations could no longer be maintained, despite a 4-fold increase in mafic rock exposure, reflects overall intensifying aridification, denudation of the CPM, and a shift from dense forests to shrubby-savanna-like vegetation in Euramerica at this time. ~~Thus~~ However, given that the magmatic CO₂ flux likely increased ~~through~~ already by the ~~early~~ earliest Permian, (summarized on Fig. 2b), our model results indicate that maintaining low steady-state CO₂ concentrations during the ~~earliest Permian 10-Myr~~ CO₂ nadir would have required an increasingly greater proportion of mafic

723 rock weathering over the reference continental silicate mineral assemblage of the Pennsylvanian, possibly well beyond a 4-
724 fold increase.

725 A CO₂-forced demise of the Late Paleozoic ice age after 290 Ma is supported by the loss of continental ice from the main
726 ice depocenters in south-central Gondwana by ~~281.8 Ma ± 282.17 ± 0.9132/-0.44 Ma~~ (Griffis et al., 2018; 2019) and a 6-fold
727 drop in documented glacial deposits overall between the Sakmarian and Artinskian stages (Fig. 2b; Soreghan et al., 2019). The
728 long-term CO₂ rise through the remainder of the early Permian coincided with substantial marine and terrestrial ecosystem
729 perturbation (Fig. 3b–d; Chen and Xu, (2019)). In the marine biosphere, the uniformly low rates of global macroevolution in
730 marine organisms (brown bar on Fig. 3d) were reversed and broadly adapted and distributed genera reappeared, thus restoring
731 marine ecosystems to their pre-LPIA rates (Stanley and Powell, 2003). Pennsylvanian rugose corals (pink bar on Fig. 3d)
732 underwent a major turnover in composition to those that dominated until the End-Permian extinction and cold-adapted marine
733 bivalves and brachiopods turned over to warm-adapted forms ~~aeross the Sakmarian–Artinskian boundary (290.1 Ma; blue to~~
734 ~~red bar in Fig. 3d)~~, synchronous with the onset of the long-term increase in pCO₂ ~~(290.1 Ma; blue to red bar across the~~
735 ~~Sakmarian–Artinskian boundary on Fig. 3d; Wang et al., 2006); Clapham and James, 2008). On land, the loss of pelycosaur~~
736 families (three in the late Artinskian and four in the early Kungurian (Kemp, 2006)) coincided with CO₂ sustained at >500
737 ppm. By the close of the Kungurian and the time of highest CO₂ (740 ppm), basal synapsids largely disappeared and were
738 replaced by more derived therapsids, tetrapod diversity decreased significantly (Benton, 2012; McGhee, 2018), plant extinction
739 rates reached a level comparable to that associated with the extinction of arborescent lycopsids in the early Kasimovian
740 (Cascales-Miñana et al., 2016), and extinction/origination rates increased in fishes (Friedman and Sallan, 2012).

741

742 5 Conclusions

743 Glacial-interglacial climate cycles and large-scale ~~glacioeustasyglacioeustasy~~, as well as repeated ecosystem change,
744 analogous to that of the Pleistocene, characterized Earth’s penultimate icehouse in the late Paleozoic. The dynamic glaciation
745 history of this icehouse (the Late Paleozoic Ice Age (LPIA)) came to a close by the end of the early Permian with turnover to
746 permanent greenhouse conditions. Thus, improved constraints on how atmospheric pCO₂ evolved during the LPIA and its
747 subsequent demise is crucial for better understanding the role of greenhouse-gas forcing on Earth System processes during this

Formatted: Default Paragraph Font, Font: 12 pt, English (United Kingdom)

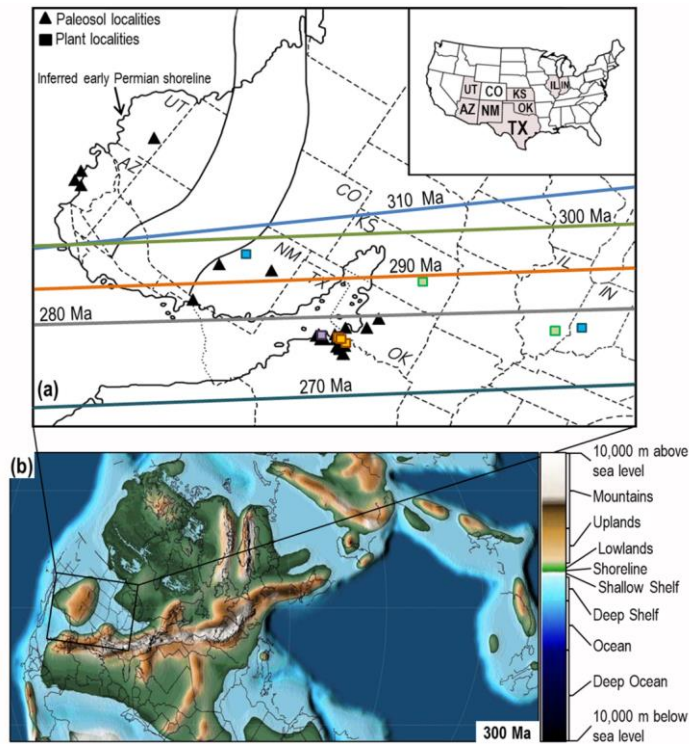
748 time. The new and age-recalibrated $p\text{CO}_2$ reconstruction presented here for a 40-Myr interval (~313 to 273 Ma) of the late
749 Paleozoic substantially refines existing Permian CO_2 estimates and provides perhaps the highest temporal resolution
750 ~~extended~~~~protracted~~ $p\text{CO}_2$ record prior to the Cenozoic. The multiproxy record confirms the previously hypothesized CO_2 -
751 glaciation linkage, including documenting the coincidence of a ~~protracted~~~~10-Myr~~ period of minimum $p\text{CO}_2$ with inferred
752 maximum ice extent during the earliest Permian. A long-term decline in $p\text{CO}_2$ through the late Carboniferous period of
753 glaciation, culminating in the earliest Permian CO_2 nadir, lends support for a ~~previously~~ modeled progressive decrease in the
754 CO_2 threshold for continental ice sheets through the LPIA.

755 Our new $p\text{CO}_2$ record provides the first stomatal-based evidence for elevated (up to 700 ppm) atmospheric CO_2
756 concentrations during short-term (10^4 -yr) interglacials. Together with new O_2 : CO_2 estimates of similar temporal resolution to
757 $p\text{CO}_2$, the new atmospheric trends indicate a close temporal relationship to repeated ecosystem restructuring in the terrestrial
758 and marine realms. In terrestrial ecosystems, the appearance and/or rise to dominance of plants with physiological and
759 anatomical mechanisms for coping with CO_2 starvation and marked aridity correspond to drops in CO_2 below 400 ppm (as low
760 as ~180 ppm) and O_2 : CO_2 ratios nearly double those of late Paleozoic background values. Similarly, decreasing rates of
761 macroevolution and diversity in the low-latitude oceans correspond to falling CO_2 to below 400 ppm. These CO_2 -ecosystem
762 relationships lead us to hypothesize that 400 ppm was an important threshold for ecosystem resilience during the late Paleozoic.

763 Modeling of steady-state $p\text{CO}_2$ during the late Paleozoic using an intermediate complexity climate-~~C~~carbon cycle model
764 (GEOCLIM) and comparison to the new multi-proxy CO_2 record provides new insight into the relative influences of ~~the~~ uplift
765 of the Central ~~Pangae~~~~an~~~~Pangean~~ Mountains, intensifying aridification, and increasing mafic-~~rock~~ to-granite rock ratio of
766 outcropping rocks on the global efficiency of CO_2 consumption and secular change in steady-state $p\text{CO}_2$ through the late
767 Paleozoic. The simulations confirm that, for the Carboniferous ~~and a continental silicate mineral assemblage for which 30%~~
768 ~~of the alkalinity generated by silicate weathering originates from the weathering of mafic rocks~~, enhanced weatherability and
769 CO_2 consumption provided by the influence of ~~the~~ ~~CPM~~uplift on surface ~~runoff~~hydrology and ~~fresh mineral supply~~erosion
770 could have lowered atmospheric $p\text{CO}_2$ well below the threshold for ice sheet initiation. Increasing the availability of mafic
771 rocks for weathering drives CO_2 levels toward snowball Earth conditions in the Carboniferous. Conversely, a substantial
772 increase (up to 4-fold) in the surface outcropping of mafic rocks over those modeled for the Carboniferous is needed to maintain

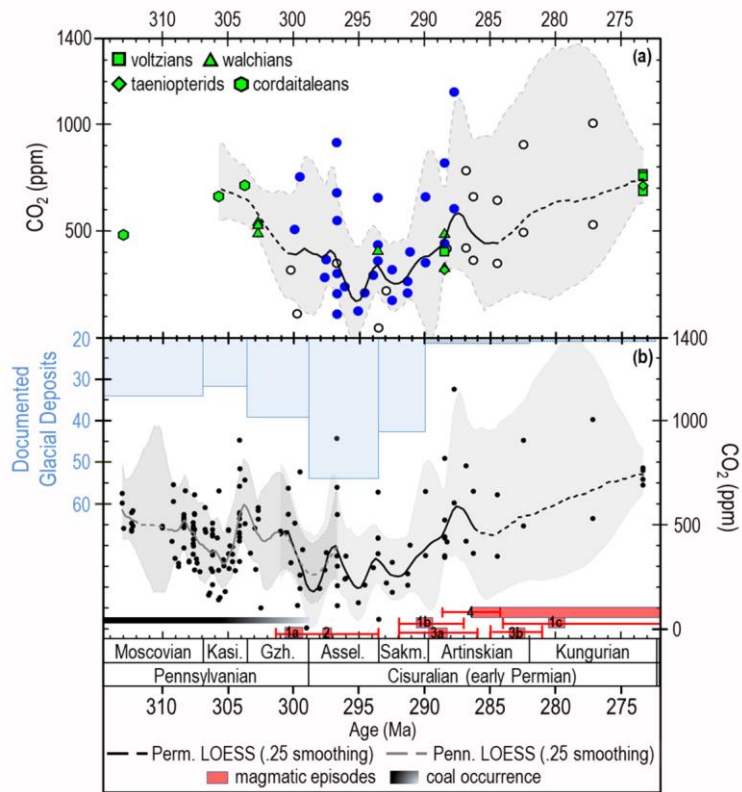
773 the 10-Myr CO₂ nadir in the earliest Permian and is compatible with maximum exhumation of the Hercynian orogenic belt at
774 this time as well as with a rapid decline in proxy-based seawater ⁸⁷Sr/⁸⁶Sr ~~inferred from biologic proxies~~. Although these
775 findings support the hypothesis of atmospheric pCO₂ response to uplift of the CPM as the primary driver for Carboniferous
776 initiation of the LPIA (Goddéris et al., 2017), they argue for a major reorganization of the predominant surface factors
777 influencing weatherability in the tropics ~~occurred~~ across the Carboniferous-Permian ~~transition leading to decreased~~ in order for
778 pCO₂ to values to have fallen to well below ~~200~~300 ppm. The demise of the LPIA was greenhouse gas-forced, reflecting the
779 increasing importance of magmatic degassing and likely decreased weathering efficiency driven by intensifying aridification,
780 denudation of the CPM, and the loss of the wetland forests throughout tropical Euramerica.

781 **Figures**



782

783 **Figure 1: Sampling localities in present-day and late Paleozoic geographic context.** (a) Sampling locations of pedogenic
 784 carbonates and plant fossils and their position relative to the Late Pennsylvanian (310 & 300 Ma) and early Permian (290 to
 785 270 Ma) equator (the colors of the flora localities correspond to that of the paleo-equator at that time). White band traversing
 786 NM and CO is the area of inferred shortening during the Laramide and Sevier orogenies. Map modified from Montañez et al.,
 787 (2007). (b) Earliest Permian (290 Ma) paleogeography (Scotese, 2016); shading corresponds to paleo-topographic/bathymetric
 788 scale on the right. Inset box is the location of panel (a).



789

790 **Figure 2: Late Paleozoic CO₂ estimates.** (a) New and revised (Montañez et al., 2007) pCO_2 estimates, bootstrapped LOESS

791 trend, and 75% confidence interval (CI). Revised pedogenic carbonate-based estimates were made using $\delta^{13}C_{OOM}$ (blue filled

792 circles; $n = 28$; Fig. S1) and $\delta^{13}C_{POM}$ (open black circles; $n = 16$; Fig. S1). Trendline is the median of 1000 bootstrapped LOESS

793 analyses; dashed intervals indicate low data density and higher uncertainty. See Material and Methods for details, Fig. S1 for

794 error bars on individual CO₂ estimates and the 95% CI, and Richey et al. (2020); <https://doi.org/10.25338/B8S90Q> for the full

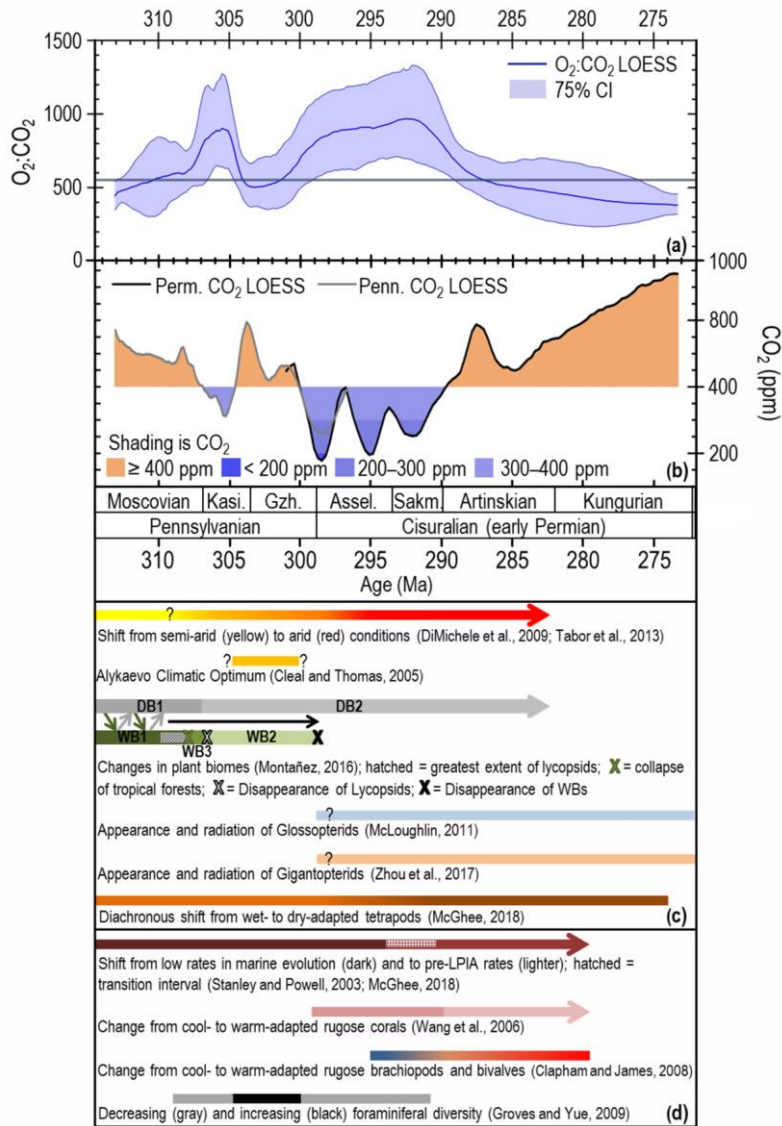
795 dataset. (b) Multiproxy CO₂ record and individual estimates (this study and age-recalibrated values of Montañez et al., (2016);

796 $n = 165$), documented glacial deposits (Soreghan et al., 2019), and best estimate of timing (and uncertainties) of magmatic

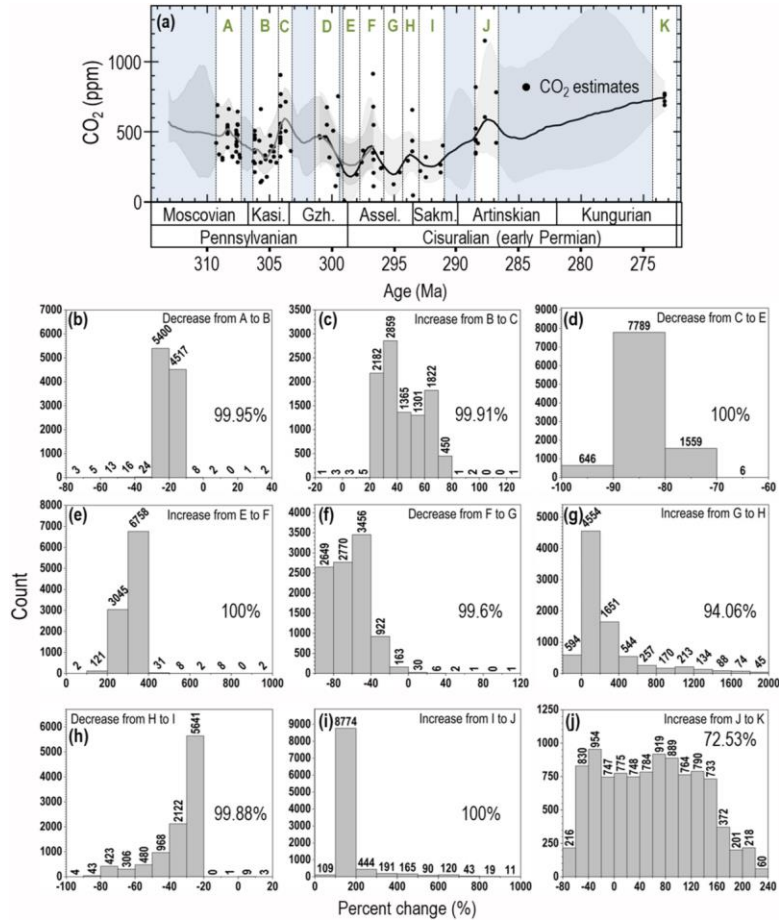
797 episodes: 1a = Tarim 1, China (~300 Ma); 1b = Tarim 2 (292–287, peak ~290 Ma); 1c = Tarim 3 (284–272, peak ~ 280 Ma;
798 Chen and Xu, (2019)); 2 = Skagerrak-centered, NW Europe (297.5 ± 3.8 Ma; Torsvik et al., (2008)); 3a = Panjal Traps, NW
799 India (289 ± 3 Ma; Shellnutt, (2018)); 3b = Qiangtang Traps, Tibet (283 ± 2 Ma; Zhai et al., (2013)); 4 = Choiyoi, W Argentina
800 (beginning $286.5 \text{ Ma} \pm 2.3$ Ma, continuing for up to 39 Myr; Sato et al., (2015)). Trendlines as in (A); dashed intervals across
801 the Carboniferous-Permian boundary (298.9 Ma) indicates overlap of the two LOESS trendlines.

802

803



805 **Figure 3: Late Paleozoic O₂:CO₂ and pCO₂, and comparison to environmental and biotic events.** (a) O₂:CO₂ estimates
806 using CO₂ values of this study and averaged time-equivalent modeled O₂ (Krause et al., 2018; Lenton et al., 2018). Trendline
807 is the median of 1000 bootstrapped LOESS analyses; gray horizontal line is present-day O₂:CO₂. (b) Bootstrapped
808 Pennsylvanian and Permian LOESS analyses (From Fig. 2A), with significant overlap across the Pennsylvanian- Permian
809 boundary interval, ~~shaded to indicate CO₂ ranges.~~ The shading indicates CO₂ above (orange) and below (shades of blue) the
810 mean value for the 16-million-year record through the late Pennsylvanian reported in Montañez et al., (2016). Temporal
811 changes in terrestrial (c) and marine (d) ecosystems. Plant biomes from Montañez (2016): Wetland Biome (WB) 1 (i.e.,
812 lycopsid-dominated), WB 2 (i.e., cordaitalean/lycopsid co-dominance), WB 3 (i.e., tree fern-dominated), Dryland Biome (DB)
813 1 (i.e., cordaitalean-dominated), DB 2 (i.e., walchian-dominated). Diagonal arrows indicate 10⁵-yr glacial-interglacial shifts
814 between wet- and dry-adapted floras.



815

816 **Figure 4: Analysis of the statistical significance of short-term CO₂ fluctuations.** (a) White intervals (A—K) delineate
 817 short-term highs/low in the CO₂ LOESS trend used for binning (n=11; bins ±0.5 to 1 Myr resolution). Raw stomatal- and
 818 pedogenic carbonate-based CO₂ estimates generated by Monte Carlo analysis (10,000 model runs per CO₂ estimate; data in
 819 shaded intervals were not used). CO₂ between bins was compared by calculating the mean of the lowest through 10,000th

820 (highest) Monte Carlo values for all CO₂ points in each bin and comparing the means of the two bins sequentially. **(b)–(h)**
821 Histograms of the percent change between each of the 10,000 Monte Carlo means of the adjacent bins. Negative values indicate
822 a decrease in value between bins, positive values, an increase. The number above each histogram bar is of the ‘percent change’
823 values represented in each bar. The percent of the 10,000 model runs that confirm a given increase or decrease in the LOESS
824 trend is indicated by the % value shown on the right side of each panel. See Materials and Methods for further details.

825

826

827

828

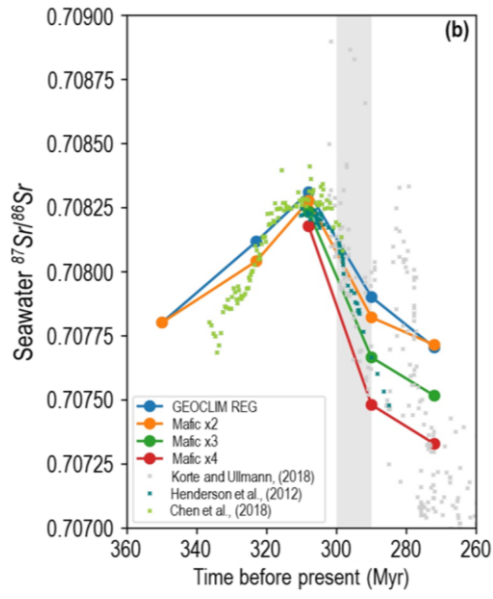
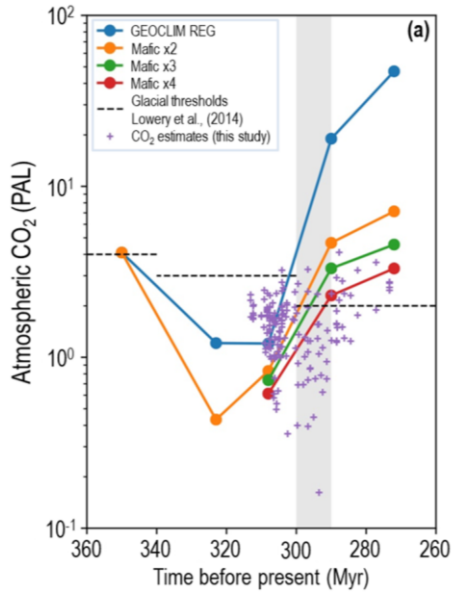
829

830

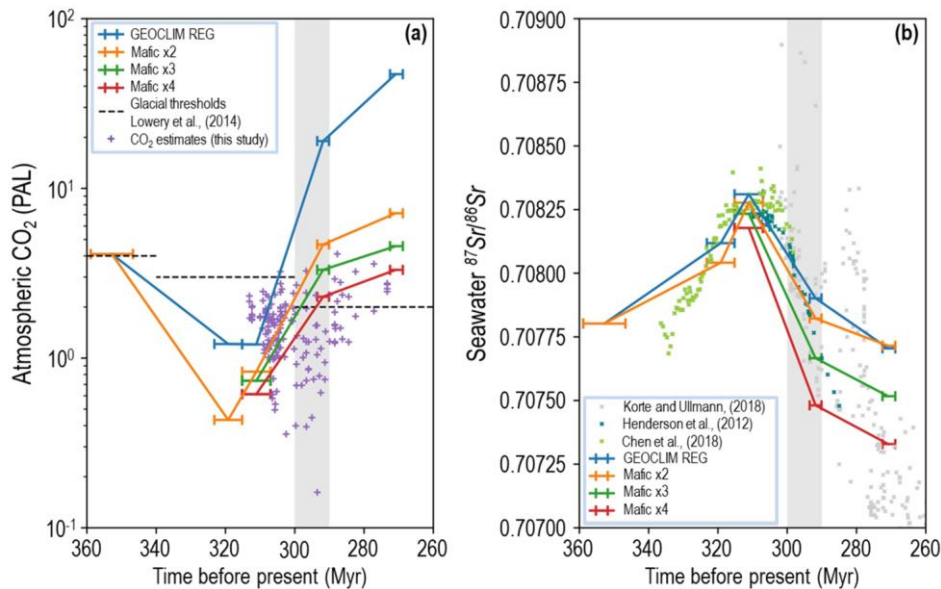
831

832

833



834



836 **Figure 5: Carboniferous through early Permian modeled (GEOCLIM) steady-state atmospheric CO₂ and seawater**
837 **⁸⁷Sr/⁸⁶Sr for different surface areas of mafic rocks available for silicate weathering.** In the model, maximum geographic
838 extent and altitude (5000 m) of the CPM is reached in the Moscovian (320 Ma), with altitude decreasing to 3000 m at 290 Ma
839 and 2000 m at 270 Ma. (a) Simulated (color symbols and lines) and proxy pCO₂ estimates (purple crosses, this study).
840 Horizontal error bars on the colored lines represent the temporal uncertainty for simulated pCO₂ estimates. CO₂ thresholds for
841 continental ice sheet initiation (360–340 Ma = 1120 ppm; 340–300 Ma = 840 ppm; 300–260 Ma = 560 ppm from Lowry et
842 al., 2014) decrease in response to equatorward drift of Gondwana, favoring an overall reduction in ice-sheet size through time.
843 The reference-reference surface area of outcropping mafic rocks² (GEOCLIM REG) maintains steady-state atmospheric CO₂
844 below the ice initiation threshold from 350 to ~304 Ma. Steady-state atmospheric CO₂ for a 2-fold, 3-fold, and 4-fold increase
845 in outcropping area of mafic rocks remains below the ice initiation threshold (560 ppm) up to ~300 Ma, crossing over at
846 progressively later times in the early Permian. Threshold cross-over of steady-state CO₂ at ~290 Ma for a 4-fold increase in
847 mafic rock exposure coincides with the termination of the 10-Myr CO₂ nadir (gray vertical bar; both panels). (b) Seawater

848 $^{87}\text{Sr}/^{86}\text{Sr}$ modeled for the same set of varying surface areas of outcropping mafic rocks and $^{87}\text{Sr}/^{86}\text{Sr}$ values of well-preserved
849 biogenic calcites (gray filled squares) and conodont bioapatites (green and blue filled squares-). Horizontal error bars on the
850 colored lines represent the temporal uncertainty for modeled Seawater $^{87}\text{Sr}/^{86}\text{Sr}$.
851

852 **Data Availability**

853 Underlying primary data is deposited in the Dryad Digital Repository (Richey et al., 2020) and can be accessed at
854 <https://doi.org/10.25338/B8S90Q>.
855

856 **Author contribution**

857 JDR and IPM designed the study. JDR collected the data, wrote the manuscript, and drafted the figures; IPM and YG carried
858 out the GEOCLIM modeling, wrote relevant parts of the manuscript, and drafted Fig. 5. All co-authors provided comments on
859 the manuscript.
860

861 **Competing interests**

862 The authors declare no competing financial interests.
863

864 **Funding**

865 This work was funded by NSF award EAR-1338281 to IPM and a National Science Foundation Graduate Research Fellowship
866 under University of California, Davis Grant #1148897 and a University of California, Davis Graduate Research Mentorship
867 Fellowship to JDR.
868

869 **Acknowledgments**

870 We thank C. Hotton (National Museum of Natural History Smithsonian Institute) and T. Taylor (~~R.I.P.~~;RIP), E. Taylor, and
871 R. Serbert (University of Kansas) for access to plant cuticle used in this study. We also thank B. Mills (University of Leeds)
872 and D. Temple-Lang and co-workers at the U.C. Davis Data Science Initiative for guidance with statistical analyses. Finally,

873 we thank J. White (Baylor University) for useful comments on the manuscript.

874

875 **References**

876 Balseiro, D., and Powell, M. G.: Carbonate collapse and the late Paleozoic ice age marine biodiversity crisis, *Geology*, 48,
877 <https://doi.org/10.1130/G46858.1>, 2019.

878 Beerling, D. J., and Berner, R. A.: Impact of a Permo-Carboniferous high O₂ event on the terrestrial carbon cycle, *Proc. Natl.*
879 *Acad. Sci. U.S.A.*, 97, 12428–12432, <https://doi.org/10.1073/pnas.220280097>, 2000.

880 Beerling, D. J., Woodward, F. I., Lomas, M. R., Wills, M. A., Quick, W. P., and Valdes, P. J.: The influence of Carboniferous
881 palaeoatmospheres on plant function: an experimental and modelling assessment, *Philos. T. Roy. Soc. Lond. B*, 353, 131–140,
882 <https://doi.org/10.1098/rstb.1998.0196>, 1998.

883 ~~Beerling, D. J., and Berner, R. A.: Impact of a Permo-Carboniferous high O₂ event on the terrestrial carbon cycle, Proc. Natl.~~
884 ~~Acad. Sci. U.S.A., 97, 12428–12432, https://doi.org/10.1073/pnas.220280097, 2000.~~

885 Belt, E. S., Heckel, P. H., Lentz, L. J., Bragonier, W. A., and Lyons, T. W.: Record of glacial–eustatic sea-level fluctuations
886 in complex middle to late Pennsylvanian facies in the Northern Appalachian Basin and relation to similar events in the
887 Midcontinent basin, *Sediment. Geol.*, 238, 79–100, <https://doi.org/10.1016/j.sedgeo.2011.04.004>, 2011.

888 Benton, M. J.: No gap in the Middle Permian record of terrestrial vertebrates, *Geology*, 40, 339–342,
889 <https://doi.org/10.1130/G32669.1>, 2012.

890 Berner, R. A., and Caldeira, K.: The need for mass balance and feedback in the geochemical carbon cycle, *Geology*, 25, 955–
891 956, [https://doi.org/10.1130/0091-7613\(1997\)025<0955:TNFMBA>2.3.CO;2](https://doi.org/10.1130/0091-7613(1997)025<0955:TNFMBA>2.3.CO;2), 1997.

892 Breecker, D. O.: Quantifying and understanding the uncertainty of atmospheric CO₂ concentrations determined from calcic
893 paleosols, *Geochem. Geophys. Geosy.*, 14, 3210–3220, <https://doi.org/10.1002/ggge.20189>, 2013.

894 Buggisch, W., Wang, X., Alekseev, A. S., and Joachimski, M. M.: Carboniferous–Permian carbon isotope stratigraphy of
895 successions from China (Yangtze platform), USA (Kansas) and Russia (Moscow Basin and Urals), *Palaeogeogr. Palaeoclimatol.*,
896 301, 18–38, <https://doi.org/10.1016/j.palaeo.2010.12.015>, 2011.

897 Cagliari, J., Philipp, R. P., Buso, V. V., Netto, R. G., Klaus Hillebrand, P., da Cunha Lopes, R., Stipp Basei, M. A., and Faccini,

898 U. F.: Age constraints of the glaciation in the Paraná Basin: evidence from new U–Pb dates, *J. Geol. Soc. London*, 173, 871–
899 874, <https://doi.org/10.1144/jgs2015-161>, 2016.

900 Cascales-Miñana, B., Diez, J. B., Gerrienne, P., and Cleal, C. J.: A palaeobotanical perspective on the great end-Permian biotic
901 crisis, *Hist. Biol.*, 28, 1066–1074, <https://doi.org/10.1080/08912963.2015.1103237>, 2016.

902 Caves, J. K., Jost, A. B., Lau, K. V., and Maher, K.: Cenozoic carbon cycle imbalances and a variable weathering feedback,
903 *Earth Planet. Sci. Lett.*, 450, 152–163, <https://doi.org/10.1016/j.epsl.2016.06.035>, 2016.

904 Chen, J., Montañez, I. P., Qi, Y., Shen, S., and Wang, X.: Strontium and carbon isotopic evidence for decoupling of $p\text{CO}_2$
905 from continental weathering at the apex of the late Paleozoic glaciation, *Geology*, 46, 395–398,
906 <https://doi.org/10.1130/G40093.1>, 2018.

907 Chen, J., and Xu, Y.-g.: Establishing the link between Permian volcanism and biodiversity changes: Insights from geochemical
908 proxies, *Gondwana Res.*, 75, 68–96, <https://doi.org/10.1016/j.gr.2019.04.008>, 2019.

909 [Chen, J., Chen, B., and Montañez, I. P.: Carboniferous isotope stratigraphy, in: *The Carboniferous Timescale*, edited by: Lucas,](#)
910 [S. G., Schneider, J. W., Wang, X., and Nikolaeva, S., Geological Society of London, London, in press.](#)

911 Clapham, M. E., and James, N. P.: Paleocology Of Early–Middle Permian Marine Communities In Eastern Australia:
912 Response To Global Climate Change In the Aftermath Of the Late Paleozoic Ice Age, *Palaios*, 23, 738–750,
913 <https://doi.org/10.2110/palo.2008.p08-022r>, 2008.

914 Cleal, C. J., and Thomas, B. A.: Palaeozoic tropical rainforests and their effect on global climates: is the past the key to the
915 present?, *Geobiology*, 3, 13–31, <https://doi.org/10.1111/j.1472-4669.2005.00043.x>, 2005.

916 Crowley, T. J., and Baum, S. K.: Modeling late Paleozoic glaciation, *Geology*, 20, 507–510, [https://doi.org/10.1130/0091-7613\(1992\)020<0507:MLPG>2.3.CO;2](https://doi.org/10.1130/0091-7613(1992)020<0507:MLPG>2.3.CO;2), 1992.

918 D’Antonio, M. P., Ibarra, D. E., and Boyce, C. K.: Land plant evolution decreased, rather than increased, weathering rates,
919 *Geology*, 48, 29–33, <https://doi.org/10.1130/G46776.1>, 2019.

920 Davydov, V. I.: Precaspian Isthmus emergence triggered the Early Sakmarian glaciation: Evidence from the Lower Permian
921 of the Urals, Russia, *Palaeogeogr. Palaeoclimatol.*, 511, 403–418, <https://doi.org/10.1016/j.palaeo.2018.09.007>, 2018.

922 de Boer, H. J., Drake, P. L., Wendt, E., Price, C. A., Schulze, E.-D., Turner, N. C., Nicolle, D., and Veneklaas, E. J.: Apparent

923 Overinvestment in Leaf Venation Relaxes Leaf Morphological Constraints on Photosynthesis in Arid Habitats, *Plant Physiol.*,
 924 172, 2286–2299, <https://doi.org/10.1104/pp.16.01313>, 2016.

925 Dessert, C., Dupré, B., François, L. M., Schott, J., Gaillardet, J., Chakrapani, G., and Bajpai, S.: Erosion of Deccan Traps
 926 determined by river geochemistry: impact on the global climate and the 87Sr/86Sr ratio of seawater, *Earth Planet. Sci. Lett.*,
 927 188, 459–474, [https://doi.org/10.1016/S0012-821X\(01\)00317-X](https://doi.org/10.1016/S0012-821X(01)00317-X), 2001.

928 Dessert, C., Dupré, B., Gaillardet, J., François, L. M., and Allègre, C. J.: Basalt weathering laws and the impact of basalt
 929 weathering on the global carbon cycle, *Chem. Geol.*, 202, 257–273, <https://doi.org/10.1016/j.chemgeo.2002.10.001>, 2003.

930 Diefendorf, A. F., Leslie, A. B., and Wing, S. L.: Leaf wax composition and carbon isotopes vary among major conifer groups,
 931 *Geochim. Cosmochim. Acta*, 170, 145–156, <https://doi.org/10.1016/j.gca.2015.08.018>, 2015.

932 DiMichele, W. A., Montañez, I. P., Poulsen, C. J., and Tabor, N. J.: Climate and vegetational regime shifts in the late Paleozoic
 933 ice age earth, *Geobiology*, 7, 200–226, <https://doi.org/10.1111/j.1472-4669.2009.00192.x>, 2009.

934 DiMichele, W. A., Wagner, R. H., Bashforth, A. R., and Álvarez-Vazquez, C.: An update on the flora of the Kinney Quarry
 935 of central New Mexico (Upper Pennsylvanian), its preservational and environmental significance, in: Carboniferous–Permian
 936 transition in central New Mexico, edited by: Lucas, S. G., Nelson, W. J., DiMichele, W. A., Speilmann, J. A., Krainer, K.,
 937 Barrick, J. E., Elrick, S., and Voigt, S., New Mexico Museum of Natural History and Science, Bulletin, New Mexico Museum
 938 of Natural History and Science, Albuquerque, New Mexico, 289–325, 2013.

939 Donnadieu, Y., Goddérís, Y., Ramstein, G., Nédélec, A., and Meert, J.: A ‘snowball Earth’ climate triggered by continental
 940 break-up through changes in runoff, *Nature*, 428, 303–306, <https://doi.org/10.1038/nature02408>, 2004.

941 ~~Donnadieu, Y., Puezat, Goddérís, Y., Pierrehumbert, R., Dromart, G., Fluteau, E., Moiroud, M., Guillocheau, F., and~~
 942 ~~Deconinck, J.-F. Jacob, R.: A better ventilated ocean triggered by Late Cretaceous changes in continental configuration, *Nat-*
 943 ~~Communs~~*GEOCLIM simulation of climatic and biogeochemical consequences of Pangea breakup, *Geochem. Geophys.**
 944 *Geosv.*, 7, 10316, <https://doi.org/10.1038/ncomms10316>, 2016~~
 945 Eros, J. M., Montañez, I. P., Osleger, D. A., Davydov, V. I., Nemyrovskaya, T. I., Poletaev, V. I., and Zhykalyak, M. V.: Sequence
 946 stratigraphy and onlap history of the Donets Basin, Ukraine: insight into Carboniferous icehouse dynamics, *Palaeogeogr.*
 947 *Palaeocl.*, 313, 1–25, <https://doi.org/10.1016/j.palaeo.2011.08.019>, 2012.

Formatted: English (United States)

Formatted: Normal, Widow/Orphan control

Formatted: English (United States)

Formatted: English (United States)

Formatted: English (United States)

Formatted: English (United States)

Formatted: English (United States)

948 Falcon-Lang, H. J., Nelson, W. J., Heckel, P. H., DiMichele, W. A., and Elrick, S. D.: New insights on the stepwise collapse
949 of the Carboniferous Coal Forests: Evidence from cyclothem and coniferopsid tree-stumps near the Desmoinesian–
950 Missourian boundary in Peoria County, Illinois, USA, *Palaeogeogr. Palaeoclimatol.*, 490, 375–392,
951 <https://doi.org/10.1016/j.palaeo.2017.11.015>, 2018.

952 Feulner, G.: Formation of most of our coal brought Earth close to global glaciation, *Proc. Natl. Acad. Sci. U.S.A.*, 114, 11333–
953 11337, <https://doi.org/10.1073/pnas.1712062114>, 2017.

954 Fielding, C. R., Frank, T. D., Birgenheier, L. P., Rygel, M. C., Jones, A. T., and Roberts, J.: Stratigraphic imprint of the Late
955 Palaeozoic Ice Age in eastern Australia: a record of alternating glacial and nonglacial climate regime, *J. Geol. Soc. London*,
956 165, 129–140, <https://doi.org/10.1144/0016-76492007-036>, 2008.

957 [Fielding, C. R., Nelson, W. J., and Elrick, S. D.: Sequence stratigraphy of the late Desmoinesian to early Missourian](#)
958 [\(Pennsylvanian\) succession of southern Illinois: Insights into controls on stratal architecture in an icehouse period of Earth](#)
959 [history, *J. Sediment. Res.*, 90, 200-227, <https://doi.org/10.2110/jsr.2020.10.2020>.](#)

960 Foster, G. L., Royer, D. L., and Lunt, D. J.: Future climate forcing potentially without precedent in the last 420 million years,
961 *Nat. Commun.*, 8, 14845, <https://doi.org/10.1038/ncomms14845>, 2017.

962 Franks, P. J., Royer, D. L., Beerling, D. J., Van de Water, P. K., Cantrill, D. J., Barbour, M. M., and Berry, J. A.: New
963 constraints on atmospheric CO₂ concentration for the Phanerozoic, *Geophys. Res. Lett.*, 41, 4685–4694,
964 <https://doi.org/10.1002/2014GL060457>, 2014.

965 Friedman, M., and Sallan, L. C.: Five hundred million years of extinction and recovery: a phanerozoic survey of large-scale
966 diversity patterns in fishes, *Palaeontology*, 55, 707–742, <https://doi.org/10.1111/j.1475-4983.2012.01165.x>, 2012.

967 Gaillardet, J., Dupré, B., Louvat, P., and Allègre, C. J.: Global silicate weathering and CO₂ consumption rates deduced from
968 the chemistry of large rivers, *Chem. Geol.*, 159, 3–30, [https://doi.org/10.1016/S0009-2541\(99\)00031-5](https://doi.org/10.1016/S0009-2541(99)00031-5), 1999.

969 Gao, Z., Tian, W., Wang, L., Shi, L., and Pan, M.: Emplacement of intrusions of the Tarim Flood Basalt Province and their
970 impacts on oil and gas reservoirs: A 3D seismic reflection study in Yingmaili fields, Tarim Basin, northwest China,
971 *Interpretation*, 5, SK51–SK63, <https://doi.org/10.1190/INT-2016-0165.1>, 2017.

972 Gerhart, L. M., and Ward, J. K.: Plant responses to low [CO₂] of the past, *New Phytol.*, 188, 674–695,

973 <https://doi.org/10.1111/j.1469-8137.2010.03441.x>, 2010.

974 Gibbs, M. T., Bluth, G. J., Fawcett, P. J., and Kump, L. R.: Global chemical erosion over the last 250 my; variations due to
975 changes in paleogeography, paleoclimate, and paleogeology, *Am. J. Sci.*, 299, 611-651, [https://doi.org/10.2475/ajs.299.7-](https://doi.org/10.2475/ajs.299.7-9.611)
976 9.611, 1999.

977 Glasspool, I., Scott, A., Waltham, D., Pronina, N., and Shao, L.: The impact of fire on the Late Paleozoic Earth system, *Front.*
978 *Plant Sci.*, 6, <https://doi.org/10.3389/fpls.2015.00756>, 2015.

979 Godd ris, Y., Donnadieu, Y., Le Hir, G., Lefebvre, V., and Nardin, E.: The role of palaeogeography in the Phanerozoic history
980 of atmospheric CO₂ and climate, *Earth-Sci. Rev.*, 128, 122–138, <https://doi.org/10.1016/j.earscirev.2013.11.004>, 2014.

981 Godd ris, Y., Donnadieu, Y., Carretier, S., Aretz, M., Dera, G., Macouin, M., and Regard, V.: Onset and ending of the late
982 Palaeozoic ice age triggered by tectonically paced rock weathering, *Nat. Geosci.*, 10, 382–386,
983 <https://doi.org/10.1038/ngeo2931>, 2017.

984 Griffis, N. P., Mundil, R., Monta nez, I. P., Isbell, J., Fedorchuk, N., Vesely, F., Iannuzzi, R., and Yin, Q.-Z.: A new
985 stratigraphic framework built on U-Pb single-zircon TIMS ages and implications for the timing of the penultimate icehouse
986 (Paran  Basin, Brazil), *Geol. Soc. Am. Bull.*, 130, 848–858, <https://doi.org/10.1130/B31775.1>, 2018.

987 Griffis, N. P., Monta nez, I. P., Mundil, R., Richey, J. D., Isbell, J., Fedorchuk, N., Linol, B., Iannuzzi, R., Vesely, F., Mottin,
988 T., de Rosa, E., Keller, C. B., and Yin, Q.-Z.: Coupled stratigraphic and U-Pb zircon age constraints on the late Paleozoic
989 icehouse-to-greenhouse turnover in south-central Gondwana, *Geology*, 47, 1146–1150, <https://doi.org/10.1130/G46740.1>,
990 2019.

991 Grossman, E. L., Yancey, T. E., Jones, T. E., Bruckschen, P., Chuvashov, B., Mazzullo, S. J., and Mii, H.-s.: Glaciation,
992 aridification, and carbon sequestration in the Permo-Carboniferous: The isotopic record from low latitudes, *Palaeogeogr.*
993 *Palaeocl.*, 268, 222–233, <https://doi.org/10.1016/j.palaeo.2008.03.053>, 2008.

994 Groves, J. R., and Yue, W.: Foraminiferal diversification during the late Paleozoic ice age, *Paleobiology*, 35, 367–392,
995 <https://doi.org/10.1666/0094-8373-35.3.367>, 2009.

996 Henderson, C. M., Wardlaw, B. R., Davydov, V. I., Schmitz, M. D., Schiappa, T. A., Tierney, K. E., and Shen, S.: Proposal
997 for base-Kungurian GSSP, *Permophiles*, 56, 8–21, 2012.

998 Hernandez-Castillo, G. R., Stockey, R. A., Mapes, G. K., and Rothwell, G. W.: A new voltzalean conifer *Emporia royalii* sp.
999 nov. (Emporiaceae) from the Hamilton Quarry, Kansas, *Int. J. Plant Sci.*, 170, 1201–1227, <https://doi.org/10.1086/605874>,
1000 2009a.

1001 Hernandez-Castillo, G. R., Stockey, R. A., Rothwell, G. W., and Mapes, G. K.: Reconstruction of the Pennsylvanian-age
1002 walthian conifer *Emporia cryptica* sp. nov. (Emporiaceae: Voltziales), *Rev. Palaeobot. Palyno.*, 157, 218–237,
1003 <https://doi.org/10.1016/j.revpalbo.2009.05.003>, 2009b.

1004 Hernandez-Castillo, G. R., Stockey, R. A., Rothwell, G. W., and Mapes, G. K.: Reconstructing *Emporia lockardii* (Voltziales:
1005 Emporiaceae) and initial thoughts on Paleozoic conifer ecology, *Int. J. Plant Sci.*, 170, 1056–1074,
1006 <https://doi.org/10.1086/605115>, 2009c.

1007 Hibbett, D., Blanchette, R., Kenrick, P., and Mills, B.: Climate, decay, and the death of the coal forests, *Curr. Biol.*, 26, R563–
1008 R567, <https://doi.org/10.1016/j.cub.2016.01.014>, 2016.

1009 [Horton, D. E., Poulsen, C. J., Montañez, I. P., and DiMichele, W. A.: Eccentricity-paced late Paleozoic climate change,](https://doi.org/10.1016/j.palaeo.2012.03.014)
1010 [Palaeogeogr. Palaeoclimatol., 331, 150–161, https://doi.org/10.1016/j.palaeo.2012.03.014, 2012.](https://doi.org/10.1016/j.palaeo.2012.03.014)

1011 Ibarra, D. E., Caves, J. K., Moon, S., Thomas, D. L., Hartmann, J., Chamberlain, C. P., and Maher, K.: Differential weathering
1012 of basaltic and granitic catchments from concentration–discharge relationships, *Geochim. Cosmochim. Acta*, 190, 265–293,
1013 <https://doi.org/10.1016/j.gca.2016.07.006>, 2016.

1014 Ibarra, D. E., Rugenstein, J. K. C., Bachan, A., Baresch, A., Lau, K. V., Thomas, D. L., Lee, J.-E., Boyce, C. K., and
1015 Chamberlain, C. P.: Modeling the consequences of land plant evolution on silicate weathering, *Am. J. Sci.*, 319, 1–43,
1016 <https://doi.org/10.2475/01.2019.01>, 2019.

1017 Isbell, J. L., Henry, L. C., Gulbranson, E. L., Limarino, C. O., Fraiser, M. L., Koch, Z. J., Cicciooli, P. L., and Dineen, A. A.:
1018 Glacial paradoxes during the late Paleozoic ice age: Evaluating the equilibrium line altitude as a control on glaciation,
1019 *Gondwana Res.*, 22, 1–19, <https://doi.org/10.1016/j.gr.2011.11.005>, 2012.

1020 [Joshi, M. M., Mills, B. J. W., and Johnson, M.: A Capacitor-Discharge Mechanism to Explain the Timing of Orogeny-Related](https://doi.org/10.1029/2019GL083368)
1021 [Global Glaciations, *Geophys. Res. Lett.*, 46, 8347–8354, https://doi.org/10.1029/2019GL083368, 2019.](https://doi.org/10.1029/2019GL083368)

1022 Käbner, A., Tichomirowa, M., Lützner, H., and Gaupp, R.: New high precision CA-ID-TIMS U-Pb zircon ages from the

1023 Thuringian Forest Rotliegend section, in: Geophysical Research Abstracts, European Geophysical Union, Vienna, Austria,
1024 2019,

1025 Kemp, T. S.: The origin and early radiation of the therapsid mammal-like reptiles: a palaeobiological hypothesis, *J. Evolution.*
1026 *Biol.*, 19, 1231–1247, <https://doi.org/10.1111/j.1420-9101.2005.01076.x>, 2006.

1027 Koch, J. T., and Frank, T. D.: The Pennsylvanian–Permian transition in the low-latitude carbonate record and the onset of
1028 major Gondwanan glaciation, *Palaeogeogr. Palaeoclimatol.*, 308, 362–372, <https://doi.org/10.1016/j.palaeo.2011.05.041>, 2011.

1029 Korte, C., and Ullmann, C. V.: Permian strontium isotope stratigraphy, *Geol. Soc. Spec. Publ.*, 450, 105–118,
1030 <https://doi.org/10.1144/sp450.5>, 2018.

1031 Krause, A. J., Mills, B. J. W., Zhang, S., Planavsky, N. J., Lenton, T. M., and Poulton, S. W.: Stepwise oxygenation of the
1032 Paleozoic atmosphere, *Nat. Commun.*, 9, <https://doi.org/10.1038/s41467-018-06383-y>, 2018.

1033 Lee, C.-T. A., Thurner, S., Paterson, S., and Cao, W.: The rise and fall of continental arcs: Interplays between magmatism,
1034 uplift, weathering, and climate, *Earth Planet. Sci. Lett.*, 425, 105–119, <https://doi.org/10.1016/j.epsl.2015.05.045>, 2015.

1035 Lee, C.-T. A., and Dee, S.: Does volcanism cause warming or cooling?, *Geology*, 47, 687–688,
1036 <https://doi.org/10.1130/focus072019.1>, 2019.

1037 Lenton, T. M., Daines, S. J., and Mills, B. J. W.: COPSE reloaded: An improved model of biogeochemical cycling over
1038 Phanerozoic time, *Earth-Sci. Rev.*, 178, 1–28, <https://doi.org/10.1016/j.earscirev.2017.12.004>, 2018.

1039 Li, H., Taylor, E. L., and Taylor, T. N.: Permian Vessel Elements, *Science*, 271, 188–189,
1040 <https://doi.org/10.1126/science.271.5246.188>, 1996.

1041 Lowry, D. P., Poulsen, C. J., Horton, D. E., Torsvik, T. H., and Pollard, D.: Thresholds for Paleozoic ice sheet initiation,
1042 *Geology*, 42, 627–630, <https://doi.org/10.1130/G35615.1>, 2014.

1043 Macdonald, F. A., Swanson-Hysell, N. L., Park, Y., Lisiecki, L., and Jagoutz, O.: Arc-continent collisions in the tropics set
1044 Earth’s climate state, *Science*, 364, 181–184, <https://doi.org/10.1126/science.aav5300>, 2019.

1045 Maher, K., and Chamberlain, C. P.: Hydrologic Regulation of Chemical Weathering and the Geologic Carbon Cycle, *Science*,
1046 343, 1502–1504, <https://doi.org/10.1126/science.1250770>, 2014.

1047 McGhee, G. R.: *Carboniferous Giants and Mass Extinction: The Late Paleozoic Ice Age World*, Columbia University Press,

1048 New York, 2018.

1049 McKenzie, N. R., Horton, B. K., Loomis, S. E., Stockli, D. F., Planavsky, N. J., and Lee, C.-T. A.: Continental arc volcanism
1050 as the principal driver of icehouse-greenhouse variability, *Science*, 352, 444–447, <https://doi.org/10.1126/science.aad5787>,
1051 2016.

1052 McLoughlin, S.: *Glossopteris*—insights into the architecture and relationships of an iconic Permian Gondwanan plant, *J. Bot.*
1053 *Soc. Bengal*, 65, 93–106, 2011.

1054 Melville, R.: *Glossopteridae, Angiospermidiae and the evidence for angiosperm origin*, *Bot. J. Linn. Soc.*, 86, 279–323,
1055 <https://doi.org/10.1111/j.1095-8339.1983.tb00975.x>, 1983.

1056 ~~Montañez, I. P.: Modern soil system constraints on reconstructing deep-time atmospheric CO₂, *Geochim. Cosmochim. Acta*,
1057 *101*, 57–75, <https://doi.org/10.1016/j.gca.2012.10.012>, 2013.~~

1058 ~~Montañez, I. P.: A Late Paleozoic climate window of opportunity, *Proc. Natl. Acad. Sci. U.S.A.*, 113, 2234–2336,
1059 <https://doi.org/10.1073/pnas.1600236113>, 2016.~~

1060 ~~Montañez, I. P. and Poulsen, C. J.: The Late Paleozoic Ice Age: An Evolving Paradigm, *Annu. Rev. Earth Pl. Sc.*, 41, 629–
1061 *656*, <https://doi.org/10.1146/annurev.earth.031208.100118>, 2013.~~

1062 ~~Montañez, I. P., Tabor, N. J., Niemeier, D., DiMichele, W. A., Frank, T. D., Fielding, C. R., Isbell, J. L., Birgenheier, L. P.,
1063 and Rygel, M. C.: CO₂-forced climate and vegetation instability during Late Paleozoic deglaciation, *Science*, 315, 87–91,
1064 <https://doi.org/10.1126/science.1134207>, 2007.~~

1065 ~~Montañez, I. P.: Modern soil system constraints on reconstructing deep-time atmospheric CO₂, *Geochim. Cosmochim. Acta*,
1066 *101*, 57–75, <https://doi.org/10.1016/j.gca.2012.10.012>, 2013.~~

1067 ~~Montañez, I. P. and Poulsen, C. J.: The Late Paleozoic Ice Age: An Evolving Paradigm, *Annu. Rev. Earth Pl. Sc.*, 41, 629–
1068 *656*, <https://doi.org/10.1146/annurev.earth.031208.100118>, 2013.~~

1069 ~~Montañez, I. P.: A Late Paleozoic climate window of opportunity, *Proc. Natl. Acad. Sci. U.S.A.*, 113, 2234–2336,
1070 <https://doi.org/10.1073/pnas.1600236113>, 2016.~~

1071 ~~Montañez, I. P., McElwain, J. C., Poulsen, C. J., White, J. D., Dimichele, W. A., Wilson, J. P., Griggs, G., and Hren, M. T.:
1072 Climate, *p*CO₂ and terrestrial carbon cycle linkages during late Palaeozoic glacial–interglacial cycles, *Nat. Geosci.*, 9, 824–~~

1073 828, <https://doi.org/10.1038/ngeo2822>, 2016.

1074 Ogg, J. G., Ogg, G., and Gradstein, F. M.: A concise geologic time scale: 2016, Elsevier, New York, 2016.

1075 Pardo, J. D., Small, B. J., Milner, A. R., and Huttenlocker, A. K.: Carboniferous–Permian climate change constrained early
1076 land vertebrate radiations, *Nat. Ecol. Evol.*, 3, 200–206, <https://doi.org/10.1038/s41559-018-0776-z>, 2019.

1077 Poulsen, C. J., Tabor, C., and White, J. D.: Long-term climate forcing by atmospheric oxygen concentrations, *Science*, 348,
1078 1238–1241, <https://doi.org/10.1126/science.1260670>, 2015.

1079 Richey, J. D., Montañez, I. P., Goddérís, Y., Looy, C. V., Griffis, N. P., and DiMichele, W. A.: Primary Data from Richey et
1080 al., 2020 (Climate~~s~~ Of The Past ~~(in review)~~), <https://doi.org/10.25338/B8S90Q>, 2020.

1081 Romanek, C. S., Grossman, E. L., and Morse, J. W.: Carbon isotopic fractionation in synthetic aragonite and calcite: Effects
1082 of temperature and precipitation rate, *Geochim. Cosmochim. Acta*, 56, 419–430, [https://doi.org/10.1016/0016-7037\(92\)90142-](https://doi.org/10.1016/0016-7037(92)90142-6)
1083 6, 1992.

1084 Sato, A. M., Llambías, E. J., Basei, M. A. S., and Castro, C. E.: Three stages in the Late Paleozoic to Triassic magmatism of
1085 southwestern Gondwana, and the relationships with the volcanogenic events in coeval basins, *J. S. Am. Earth Sci.*, 63, 48–69,
1086 <https://doi.org/10.1016/j.jsames.2015.07.005>, 2015.

1087 Scotese, C.: PALEOMAP PaleoAtlas for GPlates and the PaleoData Plotter Program, PALEOMAP Project,
1088 <https://www.earthbyte.org/paleomap-paleoatlas-for-gplates/>, 2016.

1089 Shellnutt, J. G.: The Panjal Traps, in: Large Igneous Provinces from Gondwana and Adjacent Regions, edited by: Sensarma,
1090 S., and Storey, B. C., Special Publications, 1, Geological Society, London, 59–86, 2018.

1091 Šimůnek, Z.: Cuticular analysis of new Westphalian and Stephanian Cordaites species from the USA, *Rev. Palaeobot. Palyno.*,
1092 253, 1–14, <https://doi.org/10.1016/j.revpalbo.2018.03.001>, 2018.

1093 Soreghan, G. S., Soreghan, M. J., and Heavens, N. G.: Explosive volcanism as a key driver of the late Paleozoic ice age,
1094 *Geology*, 47, 600–604, <https://doi.org/10.1130/G46349.1>, 2019.

1095 Spalletti, L. A., and Limarino, C. O.: The Choiyoi magmatism in south western Gondwana: implications for the end-permian
1096 mass extinction-a review, *Andean Geol.*, 44, 328–338, <http://dx.doi.org/10.5027/andgeoV44n3-a05>, 2017.

1097 Srivastava, A. K.: Evolutionary tendency in the venation pattern of Glossopteridales, *Geobios*, 24, 383–386,

1098 [https://doi.org/10.1016/S0016-6995\(06\)80235-4](https://doi.org/10.1016/S0016-6995(06)80235-4), 1991.

1099 Stanley, S. M.: ~~Estimates~~, and Powell, M. G.: ~~Depressed rates of origination and extinction during the late Paleozoic ice age:~~
1100 ~~a new state for the global~~ magnitudes of major marine ecosystem, *Geology*, 31, 877–880 mass extinctions in earth history, *Proc.*
1101 *Natl. Acad. Sci. U.S.A.*, 113, E6325–E6334, <https://doi.org/10.1130/G19654R.1>, 2003/1073/pnas.1613094113, 2016.

1102 Stanley, S. M., and Powell, M. G.: ~~Depressed rates~~: ~~Estimates of origination and extinction during the~~ magnitudes of major ~~late~~
1103 ~~Paleozoic ice age: a new state for the global~~ marine mass extinctions in earth history, *Proc. Natl. Acad. Sci. U.S.A.*, 113,
1104 ~~E6325–E6334~~ ecosystem, *Geology*, 31, 877–880, <https://doi.org/10.1073/pnas.1613094113>, 2016/1130/G19654R.1, 2003.

1105 Tabor, N. J., and Montañez, I. P.: Oxygen and hydrogen isotope compositions of Permian pedogenic phyllosilicates:
1106 development of modern surface domain arrays and implications for paleotemperature reconstructions, *Palaeogeogr. Palaeocli.*,
1107 223, 127–146, <https://doi.org/10.1016/j.palaeo.2005.04.009>, 2005.

1108 Tabor, N. J., DiMichele, W. A., Montañez, I. P., and Chaney, D. S.: Late Paleozoic continental warming of a cold tropical
1109 basin and floristic change in western Pangea, *Int. J. Coal. Geol.*, 119, 177–186, <https://doi.org/10.1016/j.coal.2013.07.009>,
1110 2013.

1111 Torsvik, T. H., Smethurst, M. A., Burke, K., and Steinberger, B.: Long term stability in deep mantle structure: Evidence from
1112 the ~300 Ma Skagerrak-Centered Large Igneous Province (the SCLIP), *Earth Planet. Sci. Lett.*, 267, 444–452,
1113 <https://doi.org/10.1016/j.epsl.2007.12.004>, 2008.

1114 Walker, J. C. G., Hays, P. B., and Kasting, J. F.: A negative feedback mechanism for the long-term stabilization of
1115 Earth's surface temperature, *J. Geophys. Res.-Oceans*, 86, 9776–9782, <https://doi.org/10.1029/JC086iC10p09776>,
1116 1981.

1117 Wang, X.-D., Wang, X.-J., Zhang, F., and Zhang, H.: Diversity patterns of Carboniferous and Permian rugose corals in South
1118 China, *Geol. J.*, 41, 329–343, <https://doi.org/10.1002/gj.1041>, 2006.

1119 West, A. J.: Thickness of the chemical weathering zone and implications for erosional and climatic drivers of weathering and
1120 for carbon-cycle feedbacks, *Geology*, 40, 811–814, <https://doi.org/10.1130/g33041.1>, 2012.

1121 Wilson, J. P., Montañez, I. P., White, J. D., DiMichele, W. A., McElwain, J. C., Poulsen, C. J., and Hren, M. T.: Dynamic
1122 Carboniferous tropical forests: new views of plant function and potential for physiological forcing of climate, *New Phytol.*,

- 1123 215, 1333–1353, <https://doi.org/10.1111/nph.14700>, 2017.
- 1124 Wilson, J. P., White, J. D., Montañez, I. P., DiMichele, W. A., McElwain, J. C., Poulsen, C. J., and Hren, M. T.: Carboniferous
1125 plant physiology breaks the mold, *New Phytol.*, <https://doi.org/10.1111/nph.16460>, 2020.
- 1126 Yang, S., Chen, H., Li, Z., Li, Y., Yu, X., Li, D., and Meng, L.: Early Permian Tarim Large Igneous Province in northwest
1127 China, *Sci. China Earth Sci.*, 56, 2015–2026, <https://doi.org/10.1007/s11430-013-4653-y>, 2013.
- 1128 Zhai, Q.-g., Jahn, B.-m., Su, L., Ernst, R. E., Wang, K.-l., Zhang, R.-y., Wang, J., and Tang, S.: SHRIMP zircon U–Pb
1129 geochronology, geochemistry and Sr–Nd–Hf isotopic compositions of a mafic dyke swarm in the Qiangtang terrane, northern
1130 Tibet and geodynamic implications, *Lithos*, 174, 28–43, <https://doi.org/10.1016/j.lithos.2012.10.018>, 2013.
- 1131 Zhou, W., Wan, M., Koll, R. A., and Wang, J.: Occurrence of the earliest gigantopterid from the basal Permian of the North
1132 China Block and its bearing on evolution, *Geol. J.*, 53, 500–509, <https://doi.org/10.1002/gj.2907>, 2017.